2. EXPLANATORY NOTES[1]

Shipboard Scientific Party[2]

INTRODUCTION

In this chapter, we have assembled information that will help the reader understand the observations on which our preliminary conclusions are based and also help the interested investigator select samples for further analysis. This information concerns only shipboard operations and analyses described in the site reports in the *Initial Reports* volume of the Leg 170 *Proceedings of the Ocean Drilling Program.* Methods used by various investigators for shore-based analyses of Leg 170 data will be described in the individual scientific contributions to be published in the *Scientific Results* volume and elsewhere.

The separate sections of the site chapters were written by the shipboard scientific specialists for each scientific discipline (see the Shipboard Scientific Participant list at the front of this volume).

Drilling Operations

Three coring systems were used during Leg 170: the advanced hydraulic piston corer (APC), the extended core barrel (XCB), and the rotary core barrel (RCB). Any one of these systems was applied to maximize core recovery in the lithology being drilled. Drilling systems and their characteristics, such as drilling-related deformation, are summarized in the "Explanatory Notes" chapters of various previous *Initial Reports* volumes. The Leg 139 *Initial Reports* volume includes a particularly detailed description.

Drilled intervals are referred to in meters below rig floor (mbrf), which are measured from the kelly bushing on the rig floor to the bottom of the drill pipe, and meters below seafloor (mbsf), which are calculated. In the case where sediments of substantial thickness cover the seafloor (as at all sites during Leg 170), the mbrf depth of the seafloor is determined with a mudline core, assuming 100% recovery for the cored interval in the first core. Water depth is calculated by subtracting the distance from the rig floor to the sea level from the mudline measurement in mbrf. Note that this water depth usually differs from precision depth recorder (PDR) measurements by a few to several meters. The mbsf depths of core tops are calculated by subtracting the seafloor depth in mbrf from the core top depth in mbrf. The core-top datums from the driller are the ultimate depth reference for any further depth calculation procedures.

Curatorial Procedures and Sample Depth Calculations

Numbering of sites, holes, cores, and samples follows the standard Ocean Drilling Program (ODP) procedure. A full curatorial identifier for a sample consists of the following information: leg, site, hole, core number, core type, section number, and interval in centimeters measured from the top of the section. For example, a sample identification of "170-1039A-1H-1, 10–12 cm," would be interpreted as representing a sample removed from the interval between 10 and 12 cm below the top of Section 1, Core 1 (H designates that this core was taken with the APC system) of Hole 1039A during Leg 170.

In addition to the curatorial identifier, cored intervals are also assigned a depth in mbsf. The mbsf of a sample is calculated by adding the depth of the sample below the section top and the lengths of all higher sections in the core to the core-top datum measured with the drill string. A sediment core from less than a few hundred mbsf expands up to 20% upon recovery, and its length differs from the drilled interval it originates from. In addition, there is typically a coring gap between cores, as shown by composite depth construction from multiple holes performed on many previous legs. A similar discrepancy is also found between depths of core measurements and depths of corresponding logging-while-drilling (LWD) or wireline logging measurements.

Core Handling and Analysis

General core handling procedures are described in previous *Initial Report* volumes and the Shipboard Scientist's Handbook and are summarized here. As soon as cores arrived on deck, gas void samples were taken by means of a vacutainer, if applicable, for immediate analysis as part of the shipboard safety and pollution prevention program. Core-catcher samples were taken for biostratigraphic analysis. When the core was cut into sections, whole-round samples were taken for shipboard interstitial water examinations. In addition, headspace gas samples were immediately scraped from the ends of cut sections and sealed in glass vials for light hydrocarbon analysis.

Before splitting, whole-round core sections were run through the multisensor track (MST), and thermal conductivity measurements were performed on sections relevant for heat-flow studies. The cores were then split into working and archive halves, from bottom to top, so investigators should be aware that older material could have been transported upward on the split face of each section. The working half of each core was sampled for both shipboard analysis, such as physical properties, carbonate, and bulk X-ray diffraction (XRD) mineralogy, and shore-based studies. The archive half was described visually and by means of a hand-held photospectrometer and smear slides. Archive sections were run through the cryogenic magnetometer and photographed with both black-and-white and color film, a whole core at a time. Close-up photographs (black and white) were taken of particular features for illustrations in site summaries, as requested by individual scientists.

Both halves of the core were then put into labeled plastic tubes, sealed and transferred to cold storage space aboard the ship. At the end of the leg, the cores were transferred from the ship into refrigerated trucks and to cold storage at the Gulf Coast Repository of the Ocean Drilling Program.

LITHOSTRATIGRAPHY AND STRUCTURES

Visual Core Description

Visual core description included observations of composition, primary structures, deformational structures, drilling disturbance, alteration, and diagenesis on sediment and igneous rock cores. In sediments, fossils, bioturbation, and consolidation/lithification were also assessed. Observations were made macroscopically, as well as microscopically with smear slides and thin sections. Lithology determinations were based on these observations and information from car-

[1]Kimura, G., Silver, E.A., Blum, P., et al., 1997. *Proc. ODP, Init. Repts.*, 170: College Station, TX (Ocean Drilling Program).

[2]Shipboard Scientific Party is given in the list preceding the Table of Contents.

Previous Chapter Table of Contents Next Chapter

bonate measurements, XRD patterns, and X-ray fluorescence (XRF) data provided by the geochemistry laboratory. Structural measurements were conducted using both newly developed and standard orientation techniques.

The combined visual core description was captured using the application AppleCORE (by Mike Ranger, version 0.7.4f, 1989–1994), which was customized for Leg 170. In a break from practice during previous legs, we integrated sediment, igneous rock, and deformational structure descriptions into one data set presented through the AppleCORE strip log output and archived as an AppleCORE database. Graphic outputs from this application mimic the conventional ODP barrel sheet and hard rock visual core description (HRV) graphic data sheets. Testing AppleCORE was an important technical goal of Leg 170, with the objective of providing ODP with feedback in regard to its feasibility of use for routine core description on the *JOIDES Resolution* and recommendations for further necessary customizations.

Methods

Smear Slides and Lithologic Summaries

We developed a smear-slide template in Excel to store smear-slide observations (e.g., see Table 4, "Site 1039" chapter, this volume) and used a paper printout of the template to record observations while working at the microscope. Because estimates of mineral percentages from smear slides are known to be inaccurate (Rothwell, 1989), we abandoned percentage estimates entirely. Instead, we estimated relative abundances of components, using the scale A = abundant, C = common, and T = trace. After the first two sites (Sites 1039 and 1040) we amended this scale to A = abundant, C+ = very common, C = common, C– = somewhat common, and T = trace. The latter was the more useful scale and was used for the last three sites (1041, 1042, and 1043), as well as in some of the revisions of earlier tables. The smear-slide tables were reviewed for internal consistency and for correct sedimentological nomenclature where time allowed.

Another problem was how to incorporate these data into the AppleCORE database. We found it necessary to summarize and condense our observations from smear slides and place them in the context of the general appearance of the cores while the cores were still on the table. To this end, we developed a lithologic summary table, which we filled out while core description and smear-slide examination was going on, and then reviewed and amended during the report writing stage, when barrel sheets were being revised. This summary table (e.g., see Table 4, "Site 1041" chapter, this volume) proved to be an effective intermediate step between actual core observation and the production of an AppleCORE barrel sheet and was used continually on board ship to brief opposite work shifts and to cross-check the internal consistency of our observations and lithologic names. We strongly recommend the use of such running summaries to scientists on future legs.

Thin Sections

Thin sections were used to describe and classify the igneous rocks and as an aid in evaluating lithology and detailed structural relationships in selected, well-lithified sedimentary rocks. Sections were impregnated with clear epoxy before grinding and polishing to 30 µm. A standard petrographic microscope, with both transmitted and reflected light, was used for thin-section observations. Detailed descriptions of igneous rock thin sections were recorded on core section sheets and spreadsheets, which are available on CD-ROM, back pocket (this volume).

Chemical and Mineralogical Data

Carbonate analyses were routinely made on two to four samples per core (see "Geochemistry" section, this chapter). One of the carbonate samples was taken from immediately adjacent to each interstitial water sample.

XRD analyses were routinely performed on scrapings from interstitial water sediment samples. The data are archived on CD-ROM (back pocket, this volume) for post-cruise interpretation.

XRF analyses of bulk sediment samples, volcanic ashes, and igneous rocks were carried out shipboard, following standard methods (see "Geochemistry" section, this chapter), to provide constraints on lithology, provenance, and mass balance for recycling studies. Analyses of bulk sediments were carried out on squeeze-cake residues of samples chosen to provide coverage of lithologic and structural variation. Porosity measurements were made on the squeeze-cake residues to allow correction of bulk composition for the pore-water contributions of Ca, Mg, and Na. Volcanic ashes were picked from the sampling table where layers were relatively unmixed and >10 cm thick, to provide sufficient material for porosity and carbonate analysis along with the XRF. Many igneous rocks sampled for thin sections were also analyzed by XRF to aid in rock classification and to provide petrogenetic information.

Structural Measurements and Observations

Leg 170 is the latest in a series of ODP and Deep Sea Drilling Project (DSDP) legs designed to address the interaction between deformation and fluid processes at convergent plate margins. The shipboard structural geologists on Leg 156 established a standard format for recording and publishing structural geological data in ODP cores (Shipboard Scientific Party, 1995), which was adopted during Leg 170 with only minor changes, except that we used a new procedure for measuring planes and lineations found in the split cores (described below).

Structural observations were made on both the archive and working halves of the core. Commonly, scalpels and glass slides were used to gently skim away the film of mud smeared by the splitting of the core. A major problem in describing structural features in cores is distinguishing natural structures from those induced by the drilling process. Following the procedures established during Leg 156 and before, we considered a feature to be largely of natural origin if it occurred within a piece of intact core that was not broken into drilling biscuits. However, drilling-induced structures can both mimic and pass into natural structures. For instance, apparent faults with well-preserved slickensides cutting the core at an angle of 40°–60° to the long axis and indicating steep reverse movement are common in Leg 170 cores with little obvious drilling disturbance. We interpreted these apparent faults as drilling disturbances, because fractures in this orientation can be produced by the vertical loading of the drill string (Lundberg and Moore, 1986). However, some of these structures might have been localized by pre-existing natural ones.

A number of cores from apparently highly deformed zones primarily exhibit pervasive fracturing and brecciation of uncertain origin. We believe many of these zones to be naturally fractured in situ, but disaggregation of these intervals was undoubtedly exacerbated during drilling and recovery. Structural data from such intervals must be interpreted with caution. Additional artificial structural overprint occurred in material deformed plastically during core cutting with the rotary core barrel (RCB), referred to as "spiral drilling disturbance" (see "Site 1040" chapter, this volume). Although some core-scale structural features were recorded in these highly disturbed cores, caution again had to be exercised in interpreting their significance.

Each structural feature observed was recorded on a "Structural Description Sheet" (Fig. 1) based on those used on Leg 156 and before. Horizontal features have two identical interval depth values, whereas inclined structures have an interval top and bottom reference depth. The thickness of an inclined structure may deviate from the length of the interval where it occurs and was therefore documented in a separate column. The depth of occurrence below seafloor was added later for all structures as the information became available for

Leg:	Hole:	Core:	Observers:	Summary Comments:

section	depth (cm)		piece	feature	identifier	archive/	thickness	core face orientation		2nd app. orientation		Comments/Sketches
	top	base	#	#		working?		azimuth	dip/plunge	azimuth	dip/plunge	

Figure 1. “Structural Description Sheet” used for description and measurements of structural features during Leg 170.

each core. For the description of structures observed in the cores, we followed the list of structure names designed during Leg 156 (Shipboard Scientific Party, 1995), which was revised and extended from the recommendations of Lundberg and Moore (1986).

We used a newly designed tool to determine the subsurface orientation of structures (MMT: designed by M. Meschede, Fig. 2). Three steps are required to measure structures in the cores using this tool:

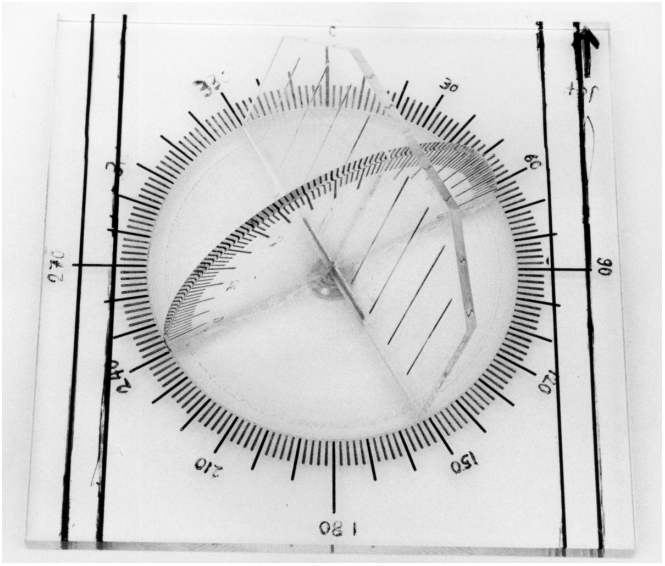

Figure 2. New tool used to measure dip azimuth and dip of planes and lines in split cores (MMT; designed by M. Meschede, Leg 170 scientific party).

1. Measure structures relative to "core face" coordinates.
2. Rotate this arbitrary reference frame into the core reference frame.
3. If possible, transform the resulting orientation to geographic coordinates and true vertical.

In step 1, the attitude of a feature was recorded according to the convention illustrated in Figure 3. The plane of the split-core face is referred to as the apparent horizontal plane. A 360° orientation net is used with a pseudo-north (000) in the upcore direction. When using the MMT, orientation of planar or linear structures was obtained in one step by holding the moveable plane parallel to the feature to be measured. The measured dip azimuth and dip angle of the fracture are recorded. Some structures were measured following the protractor method (Shipboard Scientific Party, 1995, fig. 7, p. 49). We found that measurements of single structures, particularly in soft-sediment cores, are easily obtained with both methods.

In step 2 (Fig. 3C), azimuths of planar and linear structures were rotated into the core reference frame. We used a simple PC-based rotation routine by Sperner et al. (1993). Measurements from the working half were rotated 90° counterclockwise about a horizontal east-west axis. Measurements obtained in the archive half were rotated twice, first 180° about a vertical axis, and then 90° clockwise about a horizontal east-west axis.

Finally, in step 3, the values obtained were rotated, if possible, to true azimuth and true vertical. This final rotation is possible only when paleomagnetic, multishot, or Formation MicroScanner (FMS) data are available. During Leg 170, only the first technique was possible, and in practice even this was rare. It is possible to reorient to true azimuth only those sections where unbroken individual pieces of the core of at least 10 cm length are available, or where discrete paleomagnetic samples were taken (see "Biostratigraphy and Paleo-

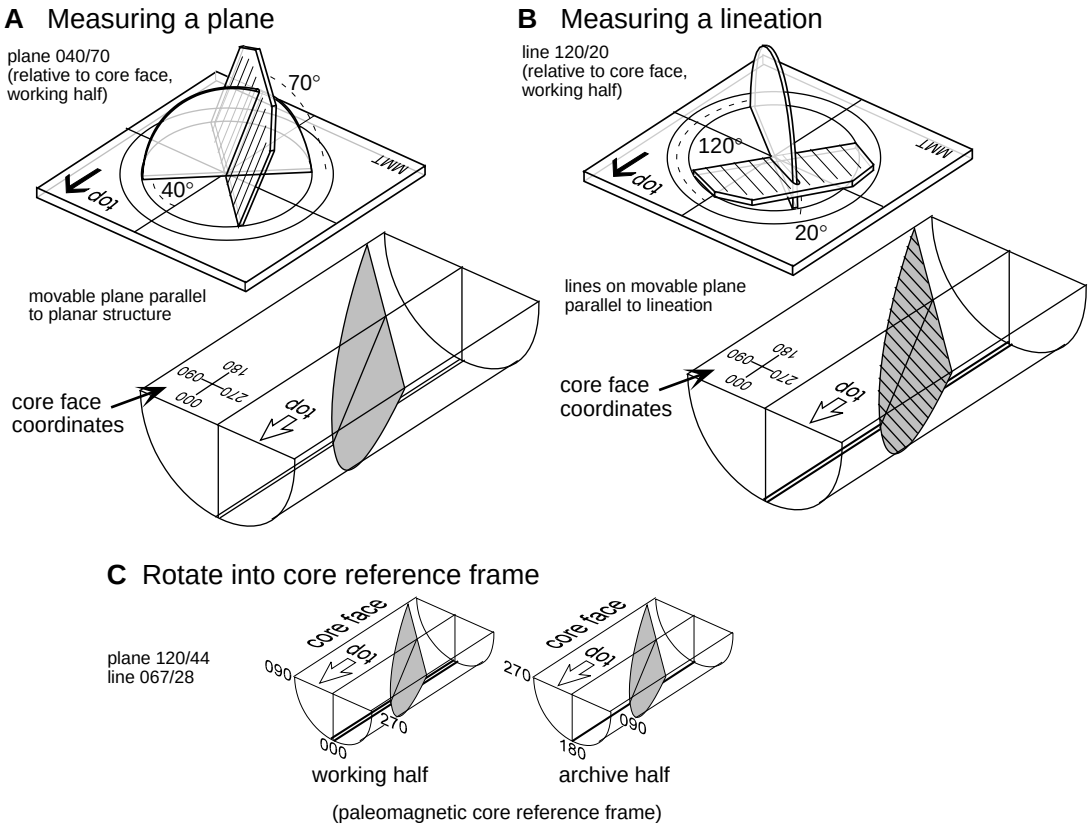

Figure 3. Conventions used for measuring azimuths and dips of structural features in cores. The core face coordinates can be seen in (**A**) and (**B**). The movable plane of the MMT was rotated until parallel with the feature to be measured. The data were recorded as dip azimuth and dip relative to the core face coordinates. These values were then rotated to the core reference frame (**C**) with pseudo-north at the bottom of the working half.

magnetism" section, this chapter). With the aid of the shipboard paleomagnetists, we were able to interpret the orientation of the natural remanent magnetism in some of the drilling biscuits for which we had structural information. The correction of data to true vertical was especially important at Site 1040, because the deviation of part of the hole from vertical was >18°. This reorientation procedure is described in detail in the "Site 1040" chapter (this volume).

Fault planes with striations were recorded with dip azimuth and dip of plane, trend and plunge of lineation, sense of movement ("+" = reverse, "–" = normal sense of movement), and a confidence level that indicates the quality of the determination of the sense of movement (1 = high confidence, 2 = very probable, 3 = possible, but not certain, and 4 = no indication; notation after Sperner et al., 1993; e.g., 063 53 008 38 – 1). To measure planar structures, particularly in soft sediments, it was sometimes necessary to cut the split core for an additional surface to get the third dimension. Using a toothpick placed parallel to the apparent dip at this second line, it was possible to define the orientation of a plane for measurement.

Structural measurements and calculations were summarized on a spreadsheet for each site. An explanation of the column headers is given in Table 1.

Classifications

Sediments and Sedimentary Rocks

Sediment classification followed the procedures outlined in Mazzulo and Graham (1988). Graphical lithology data logging and output provided by the AppleCORE program are not entirely compatible with the ternary composition scheme used for parts of that classification. However, we found that this was not a problem because, as described above, we did not estimate component percentages. Using one lithology symbol for mixtures of these components rather than a split column giving the percentage of each was therefore more appropriate.

Igneous Rocks

When describing and assigning a name to igneous rocks, the core was subdivided into lithological units based upon changes in mineralogy, texture, grain size, composition, and the occurrence of chilled margins, with the data recorded as in previous ODP *Initial Reports* volumes (e.g., Volumes 153 [Cannat, Karson, Miller, et al., 1995] and 168 [Davis, Fisher, Firth, et al., 1997]). All rocks were divided into porphyritic, aphanitic, and phaneritic groups; aphanitic rocks were subdivided into glassy, aphyric, and phyric subgroups based upon their phenocryst abundance, whereas phaneritic rocks were defined as fine (<1-mm grain size), medium (1–5 mm), and coarse grained (>5 mm). Modal abundances of primary magmatic and secondary phases were estimated visually. Rock names for intrusive rocks were assigned following the classification system of Streckeisen (1974).

At the microscopic scale, rock textures were defined according to the degree of crystallinity, with all other textural terms based on definitions in McKenzie et al. (1982). All microscopic descriptions of the core were logged on spreadsheets (see ODP *Initial Reports* Volumes 147 [Gillis, Mével, Allan, et al., 1993] and 153 [Cannat, Karson, Miller, et al., 1995] for a full discussion) and are available on the enclosed CD-ROM.

Barrel Sheet Representations Using AppleCORE

Macroscopic observations were recorded manually on core section log sheets, supplemented by smear-slide and/or thin-section observation and other data, and subsequently condensed and entered into the AppleCORE application. At the beginning of Leg 170, the program was customized to combine sedimentary and igneous rock description, deformational structures, and ODP conventions as far as possible. A long transit allowed us ample time to reflect on data presentation issues, and we agreed on a particular standard selection and arrangement of data-type columns. These data types are described below in the order that they were used.

Because we changed the use of some original AppleCORE data columns to fit Leg 170 needs (and perhaps other ODP legs), the database codes for certain data types are also different from the AppleCORE database default. This must be considered when using Leg 170 data in comparison with other AppleCORE databases. Our primary goal was not so much to create a consistent and complete database as to explore the capabilities and limitations of the application for potential routine use. After the barrel sheets were created, the output was printed as a PICT file, and headers were edited (partly on the ship, partly post cruise) to reflect the actual content of the data columns. A map of original AppleCORE data columns and their Leg 170 use is given in Table 2. Particular AppleCORE data columns were selected for specific Leg 170 data types based on plot types that are intrinsic features of AppleCORE (Table 2).

The Leg 170 configuration of the program, including patterns for lithologies, symbols, and so on, were saved in an AppleCORE custom file. This file must be installed from within the application each time the program is restarted. Barrel sheets created with a particular custom file cannot be edited or displayed properly without this step. In addition, each time the program is restarted, the strip log columns

Table 1. Explanation of structural measurement table.

Column heads	Explanation
Cr az.	Azimuth of plane in core reference frame
Cr dip	Dip of plane in core reference frame
Cr line	Azimuth of line in core reference frame
Cr l.dip	Dip of line in core reference frame
Cr sense	Sense of movement in core reference frame
Pm az.	Azimuth of plane in paleomagnetic reference frame
Pm dip	Dip of plane in paleomagnetic reference frame
Pm line	Azimuth of line in paleomagnetic reference frame
Pm l.dip	Dip of line in paleomagnetic reference frame
Sense	Sense of movement in paleomagnetic reference frame
Conf.	Confidence of movement indicator
Half	W: working half; A: archive half
Tool	Tool used for measurement
MMT	Tool designed by Martin Meschede
Protr.	Protractor

Table 2. Map of default AppleCORE data columns and use of data columns on Leg 170.

AppleCORE default	Leg 170 usage	Plot type
Meters	Depth (meters below core top)	Scale
Core and box	Core (always = 1) and section	Boxes
Clay percentage		Curve
X-Y plot 1		Curve
X-Y plot 2		Curve
Grain size		Curve
Texture		Curve
Grain size	Graphic lithology	Pattern plot
Bioturbation intensity	Alteration	Gray scale plot
Physical structures	Primary structures	Symbol/abundance plot
Accessories	None (incl. in prim. struc. or fossils)	Symbol/abundance plot
Ichnofossils	None (included in fossils)	Symbol/abundance plot
Fossils	Fossils	Symbol/abundance plot
Porosity		Gray scale plot
Pore type		Symbol/abundance plot
Stain		Gray scale plot
Hydrocarbon shows		Symbol/abundance plot
Sorting		Curve
Roundness		Curve
Samples	Samples	Text plot
Color		Text plot
Diagenesis	Diagenesis	Symbol/abundance plot
Fractures	Deformational structures	Symbol/abundance plot
Consolidation	Drilling disturbance	Gray scale plot
Fissility	Consolidation/lithification	Gray scale plot
Facies		Text plot
Facies association		Text plot
Depositional environment		Text plot
Depositional complex		Text plot
Remarks	Remarks	Text plot

desired for display must be reselected, as the display selection specifications are not stored in the custom file. It is therefore important that the program be configured at the beginning of a leg to accommodate the needs for all sites to be described. Taken a step further, it will be necessary to configure the program to accommodate the needs for all drilling sites ODP may encounter if the core description database is to be consistent from leg to leg. The following is a description of data types (columns) used on Leg 170.

Meter Scale, Core Number, and Section Number

Each core was logged in a separate file. Numbers of sections and their respective lengths were taken from the core tracking sheets and entered into a newly created barrel sheet in the "log header" window ("box tally" and "box depths"). Because a new log was begun for each core, the original core number was always 1, but it was edited post cruise to show the actual core number. The core header (site, hole, core number, and cored interval) was entered into the "well name" box (e.g., Site 1042, Hole B, Core 8R - Cored: 381.20–390.80 mbsf). The most effective way to enter a new data set was to modify an existing core log (usually the previous one) and save it with a different (subsequent) file name.

Graphic Lithology

Graphic lithology of recovered material is entered on the computer using patterns from three lithotype palettes: a modified "Clastic Lithology" palette; a modified "Carbonate Lithology" palette; and a custom igneous lithology palette. We used most original lithotypes and patterns from the AppleCORE sediment palettes, adding mainly oozes, and defined some igneous lithologies (Fig. 4). We used the "Interbedded" feature, which allows display of two lithotypes as alternating beds of program-specified thickness. We did not use the "Facies Contact" feature, because bedding boundaries are part of the "Primary Structures" column.

As mentioned above, the AppleCORE graphic display scheme is not entirely compatible with the sediment classification scheme in the ODP Shipboard Scientist's Handbook (Mazzullo and Graham, 1988); we found that this was not a significant problem. Lithologic names are given precisely in the "Remarks" column. Where an interval of sediment or sedimentary rock was a mixture of lithologic components, we chose the graphic representation of the main component. Minor constituents are not shown in the graphic lithology column, which results in greater clarity of the graphic representation. Lithologic details are shown in the other columns.

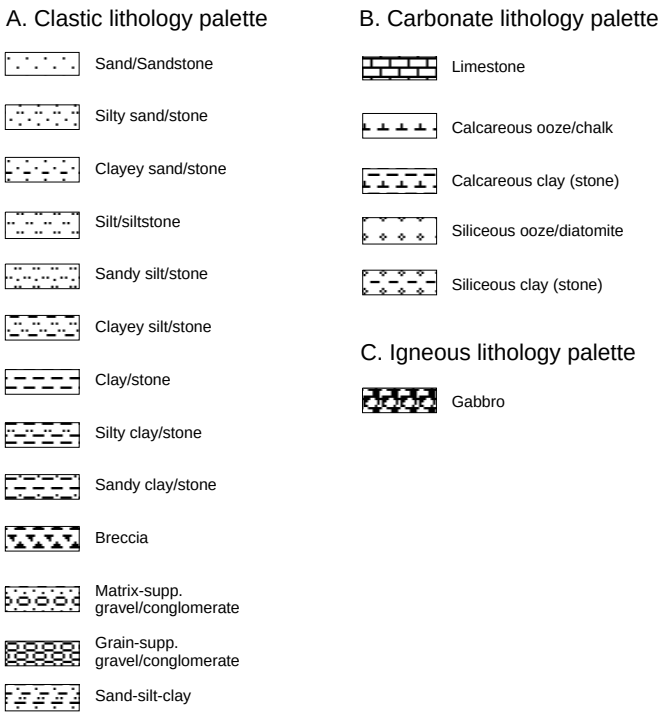

Figure 4. Patterns and symbols used for lithology, abundance, structural features, fossils, and bioturbation in AppleCORE during Leg 170.

Alteration

The alteration column represents a qualitative estimate of visible chemical alteration intensity affecting the sediment or igneous rock. The gray-scale plot reserved for bioturbation intensity in AppleCORE was used for this purpose. Figure 5 shows the five gray-scale categories for alteration as well as for two other data types described below.

Primary Structures

Primary structures are somewhat edited from the original "Physical Structures" column in AppleCORE. They are grouped in five informal categories for the purpose of creating a convenient workspace: contacts, laminations, bedding, various accessories, and igneous textures. Existing symbols were rearranged, and new ones were added (Fig. 6). Primary structures, and other data types using symbol plot types, are associated with graphical bars representing relative abundance over the chosen interval (Fig. 7).

Fossils

The AppleCORE default column for fossils was used, but we added symbols for ichnofossils here. Symbols for bioturbation were also included. We created six informal categories for workspace convenience by moving and creating symbols. These categories are microfossils, fossil fragments, macrofossils, fish fossils, trace fossils, and bioturbation (Fig. 6). Microfossil abundance was based on smear-slide descriptions.

Samples

Locations of all samples taken for shipboard analysis were entered in the "Samples" column on the core description interface. The selection list of the original AppleCORE "Sample" column was easily modified to include all ODP sample types:

SS = Smear slide,
CAR = Carbonate,
XRD = X-ray diffraction,
XRF = X-ray fluorescence,
THS = Thin section,
BIO = Biostratigraphy,
PH = Close-up photo,

	Alteration	Drilling disturbance	Lithification
Extreme	75-100%	Flow-in; Rubble and slurry	Lithified
Strong	50-75%	Disruption, contortion; Biscuits and slurry	Consolidated
Moderate	25-50%	Some contortion, bending; Strongly fractured	Firm
Weak	1-25%	Bending of layers; Slightly fractured	Soft
None	0%	None	Soupy
Not indicated			

Figure 5. Gray-scale patterns for three data types used with customized AppleCORE visual core description program.

IW = Interstitial water whole round,
WR = Other whole round, and
SAM = Other sample.

Diagenesis

Diagenetic features are subdivided into four informal categories: diagenetic minerals, nodules and concretions, cements, and miscellaneous diagenetic features (Fig. 6). Some igneous features are included in the "miscellaneous" category. The original "Diagenesis" column of AppleCORE was used for this purpose.

Deformational Structures

The "Deformational structures" column ("Fractures" column in AppleCORE) was subject to particularly intense editing during Leg 170, both because of the importance of structures to the objectives of the leg and the lack of formal definition of structural features in ODP procedures. Leg 170 usage is based on Leg 146, Cascadia Margin (Westbrook, Carson, Musgrave, et al., 1994), and Leg 156, northern Barbados Ridge (Shipley, Ogawa, Blum, et al., 1995). Leg 156 provided the main reference for graphic representation of the structures and for their working definitions (Fig. 6).

Drilling Disturbance

Deformation and disturbance of sediment that clearly results from the coring process are illustrated in the "Drilling disturbance" column in five qualitative categories (Fig. 5). The "Consolidation" gray-scale plot column of AppleCORE was used for convenience.

Consolidation/Lithification

Lithification of sediments was estimated in a qualitative way (Fig. 5). The "Fissility" gray-scale plot column of AppleCORE was used for convenience.

Remarks

The lithologic description of each core was entered as a "remark" at the very top of the core. For sediments and sedimentary rocks we subdivided between major and minor lithology (or lithologies) according to the generally used classification outlined in Mazzullo and Graham (1988).

Core Section Sheets

Data logged in AppleCORE to produce barrel sheets can also be used at an increased scale as core section sheets, mimicking the conventional ODP presentation of HRV descriptions. Hand-drawn diagrams of the archive half of the core sections were digitized using a line scanner and pasted onto a PICT format output of the AppleCORE log. The results are core section representations similar to the barrel sheets, using all primary structures, alteration, and diagenetic features already logged into AppleCORE, as well as more detailed representations and thin section descriptions.

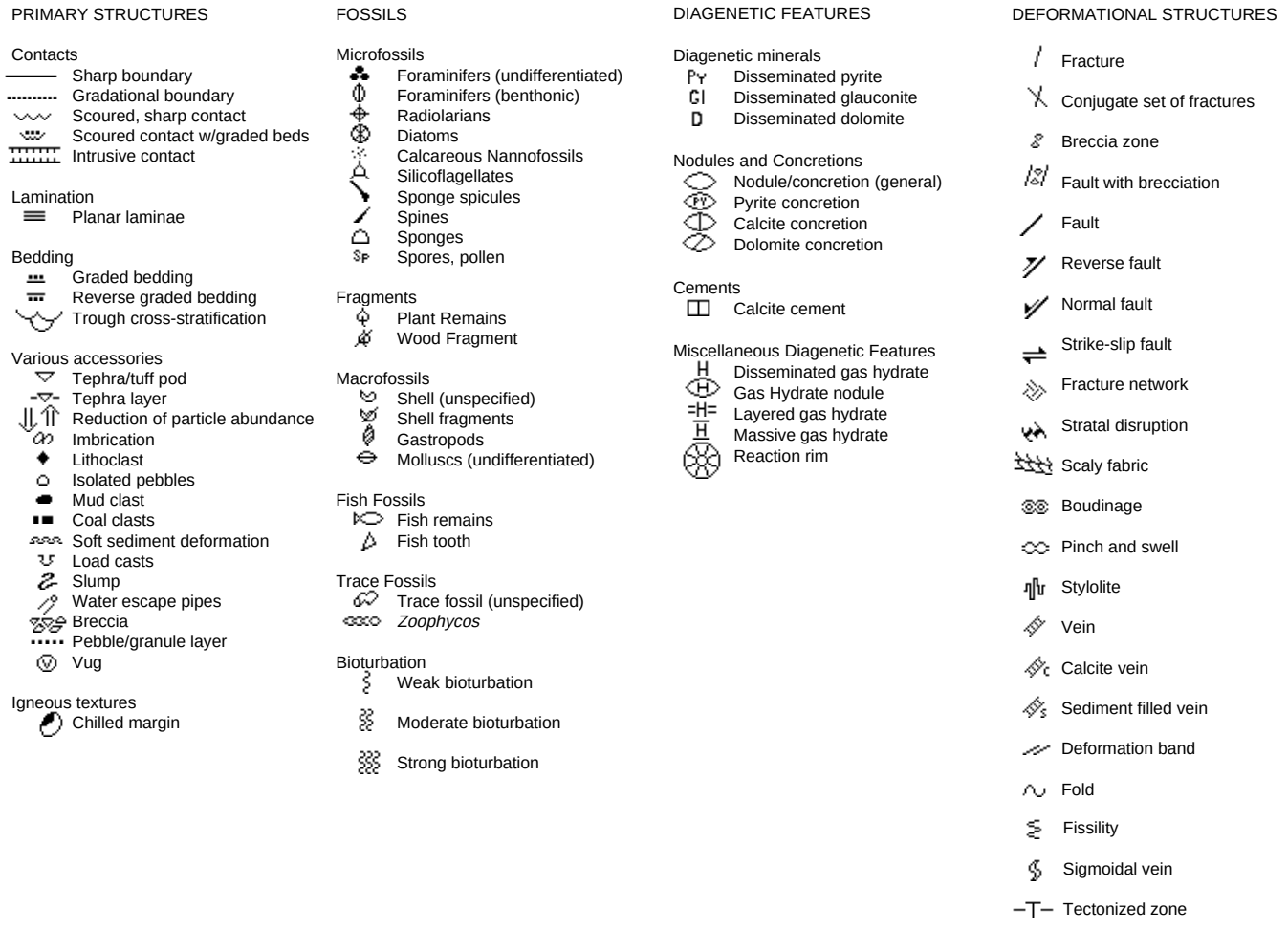

Figure 6. Symbols used with customized AppleCORE visual core description program.

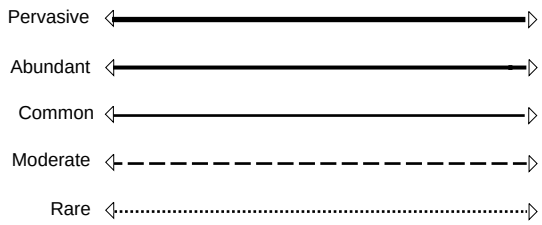

Figure 7. Abundance plots associated with symbols used with customized AppleCORE visual core description program.

Table 3. Magnetic calibration and the estimated ages of Neogene calcareous nannofossil datums used during Leg 170.

Datum	Calibration	Age (Ma)	Zone (base)
B. *Emiliania huxleyi*		0.26	CN15/NN21
T. *Pseudoemiliania lacunosa*		0.46	CN14b/NN20
T. *Helicosphaera selli*		1.47	
T. *Calcidiscus macintyrei*		1.59	
T. *Discoaster brouweri*	Olduvai	1.95	CN13a/NN19
B. A. *Discoaster triradiatus*	Matuyama	2.18	
T. *Discoaster pentaradiatus*	Matuyama	2.46-2.56	CN12d/NN18
T. *Discoaster surculus*	Matuyama	2.55-2.59	CN12c/NN17
T. *Discoaster tamalis*	Gauss	2.78	CN12b
T. *Sphenolithus* spp.	Gilbert	3.6	
T. *Reticulofenestra pseudoumbilicus*	Gilbert	3.75	CN12a/NN16
B. C. *Discoaster asymmetricus*	Cochiti	4.2	CN11b
T. *Amaurolithus primus*	Sidufjall	4.8	CN11a
B. *Ceratolithus rugosus*	Thvera	5.0-5.23	CN10c/NN13
B. *Ceratolithus acutus*	Gilbert	5.34	CN10b
B. *Triquetrorhabdulus rugosus*	Gilbert	5.34	CN10b
T. *Discoaster quinqueramus*	C3r	5.6	CN10a/NN12
T. *Amaurolithus amplificus*	C3A	5.9	
B. *Amaurolithus amplificus*	C3A	6.6	
B. *Amaurolithus primus*	C3A/C4	7.2	CN9b/NN11
T. *Discoaster loeblichii*	C4	7.4	
T. *Minylitha convallis*	C4	7.8	CN8a/NN10
B. *Discoaster berggreni*	C4	8.6	
B. *Discoaster loeblichii*	C4	8.7	
T. *Discoaster bollii*	C4A	9.1	CN8a/NN10
B. *Minylitha convallis*	C4A	9.3	
T. *Discoaster hamatus*	C4A	9.4	
T. *Coccolithus miopelagicus*	C5	10.8	
B. *Discoaster hamatus*	C5	10.7	CN7a/NN9
B. *Catinaster coalitus*	C5	10.9	CN6/NN8
T. *Discoaster kugleri*	C5	11.5	
B. *Discoaster kugleri*	C5A	11.8	CN5b/NN7
B. *Triquetrorhabdulus rugosus*	C5A	13.2	
T. *Sphenolithus heteromorphus*	C5AB	13.6	CN5a/NN6
T. *Helicosphaera ampliaperta*	C5B	15.6	CN4/NN5
B. *Sphenolithus heteromorphus*	C5D	18.2	CN3
T. *Sphenolithus belemnos*	C5E	18.3	CN3

Notes: B. = base, T. = top, A. = acme, C. = common. Based on the time scale of Berggren et al. (1995a, 1995b).

Table 4. Magnetic calibration and the estimated ages of Neogene planktonic foraminifer datums used during Leg 170.

Datum	Age (Ma)	Zone (base)
B. *Globorotalia hirsuta*	0.45	N23
T. *Globorotalia tosaensis*	0.65	
T. *Pulleniatina finalis*	1.4	
T. *Globigerinoides fistulosus*	1.6	
T. *Globigerinoides extremus*	1.77	
B. *Globorotalia truncatulinoides*	2.0	N22
T. *Dentoglobigerina altispira*	3.1	
T. *Sphaeroidinellopsis seminulina*	3.12	
B. *Globigerinoides fistulosus*	3.33	
B. *Globorotalia tosaensis*	3.35	N21
T. *Globorotalia margaritae*	3.58	
T. *Pulleniatina* spp. sinistral to dextral	3.95	
T. *"Globigerina" nepenthes*	4.2	
B. *Globorotalia crassaformis*	4.5	
B. *Sphaeroidinella dehiscens*	5.2	N19
B. *Globorotalia tumida*	5.6	N18
T. *Globoquadrina dehiscens*	5.8	
B. *Globorotalia margaritae*	6.0	
T. *Globorotalia lenguaensis*	6.0	
B. *Pulleniatina primalis*	6.4	N17b
B. *Globorotalia conomiozea*	7.12	
B. *Globorotalia cibaoensis*	7.8	
B. *Candeina nitida*	8.1	
B. *Globorotalia juani*	8.1	
B. *Globigerinoides extremus*	8.3	
B. *Globorotalia plesiotumida*	8.3	N17a
B. *Neogloboquadrina humerosa*	8.5	
B. *Neogloboquadrina acostaensis*	10.9	N16
T. *Neogloboquadrina mayeri*	11.4	
T. *Globorotalia siakensis*	11.4	
B. *"Globigerina" nepenthes*	11.8	N14
T. *Globorotalia fohsi robusta*	11.9	
T. *Globorotalia praescitula*	11.9	
T. *Globorotalia fohsi lobata*	12.1	N13
B. *Globorotalia fohsi robusta*	12.3	
T. *Tenuitella cleminenciae*	12.3	
B. *Globorotalia fohsi lobata*	12.5	N12
B. *Globorotalia praefohsi*	12.7	
B. *Globorotalia fohsi* sensu stricto	12.7	N11
T. *Globorotalia peripheronda*	14.6	N10
B. *Globorotalia peripheroacuta*	14.8	
T. *Globigerinoides sicanus*	14.8	
T. *Praeorbulina glomerosa*	14.8	
B. *Orbulina suturalis*	15.1	N9
T. *Globorotalia miozea*	15.9	
B. *Praeorbulina circularis*	16.0	
B. *Globorotalia diminutus*	16.1	
B. *Praeorbulina glomerosa* s. stricto	16.1	
B. *Praeorbulina curva*	16.3	
B. *Globigerinoides sicanus*	16.4	N8
T. *Globorotalia incognita*	16.4	
B. *Globorotalia birnageae*	16.7	
B. *Globorotalia miozea*	16.7	

Notes: B. = base, T. = top. Datums are based on the time scale of Berggren et al. (1995a, 1995b).

BIOSTRATIGRAPHY AND MAGNETOSTRATIGRAPHY

Biostratigraphic Framework

Three microfossil groups were examined for biostratigraphic purposes on Leg 170: calcareous nannofossils, planktonic foraminifers, and diatoms. Age assignments were primarily made on core-catcher samples. Additional samples from within the core were studied when a core-catcher sample was inconclusive or otherwise unrepresentative of the core in its entirety.

We adhered to the Berggren et al. (1995a, 1995b) integrated magnetobiochronology and astronomical/geomagnetic Neogene time scale to provide correlation between the magnetostratigraphy and the chronological scale. Calibration of the calcareous nannofossil and planktonic foraminifer datums follows that of Berggren et al. (1995a, 1995b; Tables 3, 4). Calibration of the diatom datums follows that of Shackleton et al. (1995; Table 5). Age assignments of the standard epoch boundaries are given in Table 6.

Calcareous Nannofossils

Calcareous nannofossil assemblages were described from smear slides made from core-catcher samples of all cores drilled during Leg 170. When the core-catcher samples were barren of calcareous nannofossils, at least one sample was described within the core sections for that particular core. Smear slides were made directly from the raw sediment and were examined under crossed nicols and phase contrast transmitted light at 1000× magnification. Estimates of the abundances of individual nannofossil species on the smear slides were tabulated using the method of Hay (1970). Letters used to denote abundances are keyed to the base 10 log of the number of specimens of a taxon likely to be observed in any one field of view on the microscope, and are determined as follows:

H = Highly abundant, +2 (more than 100 specimens per field of view);
V = Very abundant, +1 (11–100 specimens per field of view);
A = Abundant, 0 (1–10 specimens per field of view);

Table 5. Magnetic calibration and the estimated ages of Neogene primary and secondary diatom datums for the equatorial Pacific Ocean that were used during Leg 170.

Datum	Chron	Age (Ma)	Zone (base)
T. *Nitzschia reinholdii*	Brunhes	0.62	*P. doliolus*
T. *Nitzschia fossilis*		0.70	
T. *Rhizosolenia praebergonii* var. *robusta*	Matuyama	1.72	A/B boundary
B. *Pseudoeunotia doliolus*	Olduvai	2.01	*N. reinholdii*
T. *Rhizosolenia praebergonii*	Olduvai	2.01	
T. *Thalassiosira convexa*	Matuyama	2.43	A/B boundary
T. *Nitzschia jouseae*	Gauss	2.78	*N. marina*
B. *Rhizosolenia praebergonii*	Gauss	3.18	
B. *Thalassiosira convexa* var. *convexa*	Gilbert	3.83	
B. *Asteromphalus elegans*	Gilbert	4.01	
T. *Nitzschia cylindrica*	Gilbert	4.87	
B. *Nitzschia jouseae*	Gilbert	5.12	*N. jouseae*
B. *Thalassiosira oestrupii*	Gilbert	5.63	
T. *Thalassiosira miocenica*	Gilbert	5.83	B/C boundary
T. *Asterolampra acutiloba*	C3An1	6.07	
T. *Nitzschia miocenica*	C3An1	6.07	
T. *Thalassiosira praeconvexa*	C3An2	6.17	A/B boundary
T. *Rossiella praepaleacea*	C3An2	6.52	
B. *Thalassiosira miocenica*	C3An2	6.54	
B. *Thalassiosira convexa* var. *aspinosa*	C3An2	6.55	*T. convexa*
B. *Thalassiosira praeconvexa*	C3An2	6.69	A/B boundary
T. *Nitzschia porteri*	C4n1	7.14	
B. *Nitzschia miocenica*	C4n1	7.27	*N. miocenica*
B. *Nitzschia reinholdii*	C4n1	7.30	
T. *Rossiella paleacea*	C4n1	7.37	
T. *Actinocyclus ellipticus* var. *javanicus*	C4n2	7.75	
T. *Thalassiosira burckliana*	C4n2	7.81	A/B boundary
B. *Nitzschia marina*		7.92	
T. *Thalassiosira yabei*	C4n3	8.17	*N. porteri*
B. *Nitzschia fossilis*		8.40	
T. *Coscinodiscus loeblichii*		8.79	
B. *Thalassiosira burckliana*	C4An1	8.84	A/B boundary
B. *Coscinodiscus loeblichii*		9.55	
T. *Denticulopis hustedtii*	C4An3	9.6	
T. *Actinocyclus moronensis*	C4An3	9.66	*T. yabei*
B. *Actinocyclus ellipticus* f. *lanceolata*		10.35	
T. *Crasepedodiscus coscinodiscus*		11.34	*A. moronensis*
T. *Cavitatus jouseana*		11.41	
B. *Hemidiscus cuneiformis*	C5n3	11.5	
B. *Coscinodiscus temperi* var. *delicata*		12.06	*C. coscinodiscus*
B. *Rossiella praepaleacea*		12.10	
T. *Actinocyclus ingens*		12.12	
T. *Cestodiscus pulchellus*		12.14	
T. *Crucidenticula nicobarica*		12.4	
T. *Coscinodiscus lewisianus*	C5An4	12.86	*C. gigas* var. *diorama*
T. *Thalassiosira tappanae*	C5ABn	13.2	
B. *Azpeitia nodulifer*	C5ABn	13.4	
T. *Cestodiscus peplum*	C5ADn	14.03	*C. lewisianus*
B. *Actinocyclus ellipticus*		14.04	
T. *Coscinodiscus blysmos*		14.34	
B. *Thalassiosira tappanae*	C5ADn	14.6	
T. *Annellus californicus*		15.0	A/B boundary
B. *Actinocyclus ingens*		15.5	
T. *Coscinodiscus lewisianus* var. *simillis*		15.7	
B. *Cestodiscus peplum*	C5Cn1	16.4	*C. peplum*
T. *Raphidodiscus marylandicus*	C5Cn2	16.49	
T. *Thalassiosira bukryi*	C5Cn3	16.7	A/B boundary
B. *Coscinodiscus blysmos*	C5Cn3	16.75	
T. *Triceratium pileus*	C5Dn1	17.8	
B. *Crucidenticula nicobarica*	C5Dn1	18.12	*C. nicobarica*

Notes: T. = top, B. = base. Datums are based on the time scale of Berggren et al. (1995a, 1995b) as presented in Shackleton et al. (1995).

Table 6. Age assignments of the standard epoch boundaries.

Epoch	Age (Ma)
Pliocene/Pleistocene	1.81
early Pliocene/late Pliocene	3.58
Miocene/Pliocene	5.32
middle Miocene/late Miocene	11.2
early Miocene/middle Miocene	16.4
Oligocene/Miocene	23.8

Note: Ages according to the time scale of Berggren et al. (1995a, 1995b).

C = Common, –1 (1 specimen per 2–10 fields of view);
F = Few, –2 (1 specimen per 11–100 fields of view); and
R = Rare, –3 (1 specimen per 101–1000 fields of view).

Abundance of reworked species are designated by lowercase letters. The following basic criteria were used qualitatively to describe the degree of preservation, dissolution, or overgrowth recrystallization of a nannofossil assemblage:

G = Good, individual specimens exhibit no dissolution or recrystallization.
M = Moderate, individual specimens yield slight evidence of dissolution (etching) and/or recrystallization.
P = Poor, individual specimens exhibit considerable dissolution and/or recrystallization, placoliths are dissolved and ragged, discoasters and sphenoliths are overgrown, and species determination is difficult and at times impossible.

The calcareous nannofossil zonation scheme of Martini (1971) was utilized based on the revised biostratigraphic time scale of Berggren et al. (1995a, 1995b) as applied to the nannofossil datums shown in Table 3.

Planktonic Foraminifers

Core-catcher samples of ~20 cm^3 were disaggregated by washing them with tap water over a 63-µm mesh sieve and then drying them. The dried samples were examined under a binocular microscope, and planktonic foraminifer species abundances were estimated using the following categories:

T = Trace (<1%);
R = Rare (2%–3%);
F = Few (3%–15%);
C = Common (15%–30%); and
A = Abundant (>30%).

The state of preservation of planktonic foraminifers is described as follows:

G = Good, >90% of the specimens unbroken;
M = Moderate, 30%–90% of the specimens showing dissolved or broken chambers; and
P = Poor, sample dominated by fragments and specimens with broken or dissolved chambers.

The zonal scheme of Blow (1969) that is widely employed in tropical regions is used here. Incorporated into this zonation are the modifications proposed by Kennett and Srinivasan (1983). Correlation of planktonic foraminifer datums with the revised geomagnetic polarity time scale of Berggren et al. (1995a, 1995b) for the Neogene is shown in Table 4.

Diatoms

Diatom-strewn slides were prepared by placing ~3 cm^3 of core-catcher material in a snap-cap vial, adding distilled water, agitating the vial, and removing part of the upper to middle suspended material with a pipette. The material from the pipette was then strewn onto a cover slip and mounted to a glass slide using Hyrax mounting media.

Strewn slides were examined in their entirety at a magnification of 500× for stratigraphic markers. Abundances of diatoms were based on the number of specimens observed per field of view at 500×. These abundances were recorded as follows:

A = Abundant (two or more specimens per field of view);
C = Common (1 specimen per field of view);
F = Few (1 specimen per each vertical transverse);
R = Rare (<1 specimen per each vertical transverse); and
B = Barren (no diatoms present).

Preservation of diatoms was determined qualitatively and recorded as follows:

G = Good, both finely silicified and heavily robust forms are present, and no alteration of frustules observed.
M = Moderate, finely silicified forms are present, but show some alteration.
P = Poor, finely silicified forms are absent or rare and fragmented, and the assemblage is dominated by robust forms.

Reworked species are designated by lowercase letters.

The Neogene diatom zonation for the equatorial Pacific used during Leg 170 is that of Baldauf and Iwai (1995). This scheme, developed during Leg 138, is a revision of that proposed by Barron (1985a, 1985b), which is partly based on the direct calibration of diatom datums to the magnetostratigraphy of Burckle (1972, 1977, 1978). We adhered to the most recent geomagnetic polarity time scale of Berggren et al. (1995a, 1995b), and the calibration of the diatom datums follows that of Shackleton et al. (1995) as listed in Table 5.

Age-Depth Plots

Age-depth plots were constructed to include all biostratigraphic and paleomagnetic datums sampled on the ship. In a second plot, a smooth curve fit (Stineman function with weight applied to current point and ±10% of the data range) was applied to all biostratigraphic datums, and the curve fit was resampled at the depths of all biostratigraphic datums. The same procedure was applied to the paleomagnetic age-depth interpretations. Age-depth rates were then calculated for each interval defined by two smoothed age-depth points. The resulting age-depth interval rate for biostratigraphic and paleomagnetic smoothed datums are plotted in the summary figures in the "Principal Results" section of each chapter.

The smoothing procedure mainly smooths the error in biostratigraphic ages caused by sampling core catchers and only few additional locations in cores. This depth error is most apparent when markers from different fossil types and very similar ages are sampled in two adjacent core catchers, which causes steep gradients in the age-depth curve as a result of sampling. The smoothed age-depth relationships are the first approximation of a more realistic model.

Paleomagnetism

Laboratory Facilities

The paleomagnetic laboratory on the *JOIDES Resolution* is equipped with two magnetometers: a pass-through cryogenic superconducting DC-SQUID rock magnetometer manufactured by 2-G Enterprises (Model 760R) and a Molspin spinner magnetometer. For demagnetization of samples, the laboratory contains an alternating field (AF) demagnetizer and a thermal demagnetizer (Models GSD-1 and TSD-1 by the Schonstedt Instrument Co.) capable of demagnetizing discrete specimens to 100 mT and 700°C, respectively. Partial anhysteretic remanent magnetization (pARM) can be imparted to discrete samples by a DTECH, Inc., PARM-2 system, consisting of two parallel coils mounted outside and on-axis with the AF-coil of the GSD-1 demagnetizer, and a control box. This device allows a bias field to be applied to a sample during AF demagnetization; the bias field can optionally be switched on only over a window of AF field intensity during the declining-field stage of the demagnetization cycle. In addition, there is an in-line AF demagnetizer, capable of 80 mT (2-G Model 2G600), included on the pass-through cryogenic magnetometer track for demagnetization of continuous sections. All demagnetization devices and magnetometers are shielded within micro-metal cylinders.

The sensing coils in the cryogenic magnetometer measure the magnetic signal over about a 10-cm interval, and the coils for each axis have slightly different response curves. The widths of the sensing regions correspond to about 100–150 cm^3 of cored material, all of which contributes to the signal at the sensors. The large volume of core material within the sensing region permits accurate determination of the remanence for weakly magnetized samples, despite the relatively high background noise related to the motion of the ship. The practical limit on the resolution of natural remanence of the core samples is often imposed by the magnetization of the core liner itself (about 0.01 mA/m = 10^{-8} emu/cm^3).

The pass-through cryogenic magnetometer and its AF demagnetizer are interfaced with a DEC Pentium computer and are controlled by a Labview program highly modified from the original SUPERMAG program, provided by 2-G Enterprises.

An Analytical Services Company (ASC) model IM-10 impulse magnetizer is also available in the magnetics laboratory for studies of the acquisition of both stepwise and saturation isothermal remanence

magnetization (IRM) by discrete samples. This unit can apply pulsed fields from 20 to 1200 mT.

Paleomagnetic Measurements

Pass-Through Magnetometer

The bulk of the paleomagnetic measurements on Leg 170 were made with the pass-through cryogenic magnetometer. Pass-through paleomagnetic measurements were routinely performed on the archive halves of core sections. The ODP core orientation scheme arbitrarily designates the X-axis as the horizontal (in situ) axis, radiating from the center of the core through the space between a double line inscribed lengthwise on the working half of each core liner (Fig. 8). The natural remanent magnetization (NRM) and remanence measurements after 5-, 10-, 15-, and 20-mT AF demagnetization were routinely measured at 2- to 5-cm intervals. The narrow response curves and new sample boats allowed for rapid demagnetization and measurement of discrete samples. Using five demagnetization steps, 14 discrete samples can be analyzed in about 20 min, which enabled a large number of discrete samples to be collected and measured during this leg.

Core Orientation

Core orientation of the APC was achieved with a Tensor tool that may be mounted on the core barrel. The Tensor tool consists of three mutually perpendicular magnetic sensors and two perpendicular gravity sensors. The information from both sets of sensors allows the azimuth and dip of the hole to be measured, as well as the azimuth of the APC core orientation double-line.

Orientation is not usually attempted for the top three cores (~30 mbsf), until the bottom-hole assembly (BHA) is sufficiently stabilized in the sediment. Core orientation by the Tensor tool was generally successful during Leg 170, with a subjective accuracy estimate of 20°–30°, and it contributed to the magnetostratigraphic interpretations. Exceptions to this typical performance are noted in the site chapters.

Reorientation of the rotated portions of RCB and XCB cores was also accomplished by using paleomagnetic results. Discrete samples, or portions of core, were AF demagnetized, and the characteristic remanence direction was calculated using principal component analysis. Following any correction for bedding tilt, the declinations of the characteristic directions were then rotated to 360° (for normal polarity) or 180° (for reversed polarity). In general, reorientation of structural data using paleomagnetic results was highly successful during Leg 170. In particular, core reorientation provided the information needed to ascertain the bearing of the hole deviation at the bottom of Hole 1040C. This was accomplished by assuming bedding in the lower (500–630 mbsf) was horizontal, and that the observed bedding tilts were caused by the 15°–20° hole deviation.

Coring Disturbance

Use of the RCB coring system produced a lithologically dependent form of coring disturbance that was particularly apparent at Site 1040. This disturbance was characterized by a continuous rotation of split-core declinations in a down-core spiral. Examination of whole cores with the liner peeled off, prior to whole-round sampling, revealed a twisted, ropy appearance. The twists correlated well with declination spirals measured on the same core. Recognition of the spiraled disturbance was easily performed by examination of the pass-though demagnetization results and enabled the demarkation of these disturbed zones within the Site 1040 cores.

Magnetostratigraphy

Whenever possible in the site chapters, we offer an interpretation of the magnetic polarity stratigraphy using the magnetic polarity time scale of Berggren et al., 1995a, 1995b. Two additional short geomagnetic features, observed with sufficient regularity, that may make useful stratigraphic markers for regional/global correlations are the Blake Event at 0.105 Ma and the Jamaica Event at 0.2 Ma in the Brunhes. For the upper part of the time scale (roughly Pliocene–Pleistocene), we use the traditional names to refer to various chrons and subchrons (e.g., Gauss and Jaramillo).

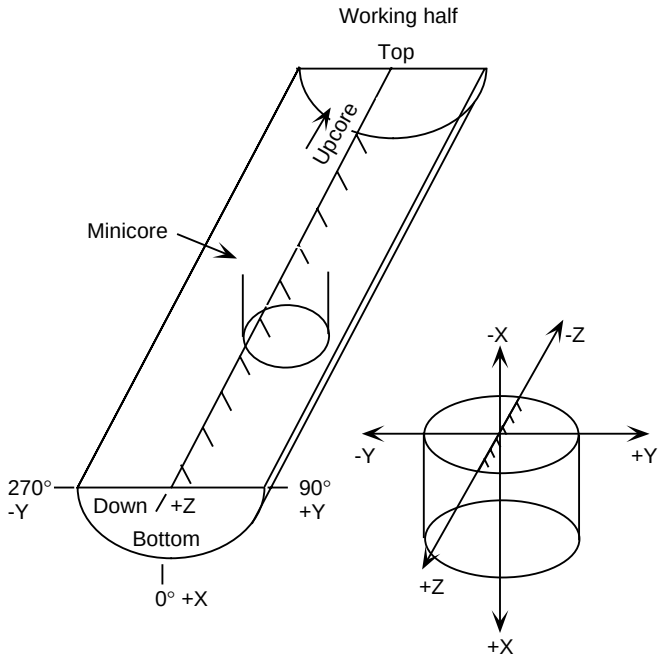

Figure 8. Core orientation conventions for split-core sections and discrete samples.

GEOCHEMISTRY

Organic Geochemistry

The shipboard organic geochemistry program for Leg 170 included (1) real-time monitoring of volatile hydrocarbon gases; (2) measurement of the inorganic carbon concentration to determine the amount of carbonate in the sediments; (3) elemental analyses of total organic carbon, total sulfur, and total nitrogen, and (4) characterization of organic matter. All instruments and methods used during Leg 170 are described below. Additional details are summarized in Emeis and Kvenvolden (1986). These analyses were performed as part of the routine shipboard safety requirements.

Hydrocarbon Gases

During Leg 170, the composition and concentration of hydrocarbons and other gases in the sediments were analyzed, usually at intervals of one per core. Two different methods, headspace and vacutainer, were used.

In the headspace method, gases released from the sediments after core recovery were analyzed by gas chromatography (GC). Immediately after retrieval on deck, a calibrated cork borer was used to obtain a defined volume of sediment from the end of a core section. Usually about a 5-cm^3 sediment sample was placed in a 21.5-cm^3 glass serum vial that was sealed with a Teflon septum and a metal crimp cap. When consolidated or lithified sediments were encountered, chips of this material were placed in the glass vial and sealed. The vial was than heated for 30 min in an oven at a constant temperature of 60°C. A 5-cm^3 volume of the gas (headspace) in the vial was extracted with a standard glass syringe for the analysis by GC.

The vacutainer method of gas collection was used where gas pockets or expansion voids were visible in the core when it was still in the core liner. A special piercing tool was used to penetrate the core liner, and an attached vacutainer or a 50-mL syringe equipped with a small three-way stopcock valve was employed to sample the gas.

Headspace and vacutainer gas samples were analyzed using a Hewlett Packard 5890 II Plus gas chromatograph equipped with a stainless steel column, packed with HaySep S (80–100 mesh) and a flame ionization detector (FID). The analyzer measures the concentrations of methane, ethane, and propane. Either the headspace syringe or the vacutainer was directly connected to the GC via a 1.0-cm^3 sample loop. Helium was used as the carrier gas, and the GC oven was held at a temperature of 90°C. The data were collected and evaluated with a Hewlett Packard 3365 Chemstation data-handling system. When higher concentrations of propane and higher hydrocarbons were suspected, gas samples were analyzed by the Natural Gas Analyzer (NGA), which measures hydrocarbons from methane to hexane. The NGA consists of a Hewlett Packard 5890 II Plus gas chromatograph equipped with a DB-1 capillary column and a FID. Nonhydrocarbon gases were analyzed at the same time via a packed column and a thermal conductivity detector (TCD). For hydrocarbon analysis, the GC oven was heated from 80°C to 100°C at 8°C/min and then to 200°C at 30°C/min. Helium was used as the carrier gas. The data collection and evaluation was done with a Hewlett Packard Chemstation data program.

Elemental Analysis

Three 2-cm^3 sediment samples were routinely taken from each core for analysis of total carbon (TC), carbonate carbon, total organic carbon (TOC), total sulfur (TS), and total nitrogen (TN).

Carbonate carbon concentrations of the samples were measured using a Coulometrics 5011 carbonate-carbon analyzer. A sample of ~10 mg of freeze-dried, ground material was reacted with 2-N HCl in the coulometer. The liberated CO_2 forms a titratable acid that, when mixed with a blue indicator solution, causes the color to fade. The color change is measured by a photodetector cell. Percentage of carbonate is calculated from the inorganic carbon (IC) content, assuming that all inorganic carbon was present as pure calcium carbonate, using the following equation:

$$(\text{Weight IC}/12) \times 100 = \text{wt\% } CaCO_3.$$

TC, TS, and TN were determined using a Carlo Erba 1500 CNS Analyzer. About 5 mg of freeze-dried, ground sediment were combusted at a temperature of 1000°C in a stream of oxygen. Using helium as a carrier gas, the oxygen was removed, and the combustion products were reduced. The reduced gases were separated by GC and quantified with a TCD. Weight percent TOC contents were calculated as the difference between weight percent TC and IC as follows:

$$\text{TOC} = \text{TC} - \text{IC}.$$

Organic Matter Type

The type of organic matter was evaluated in a selected set of samples by pyrolysis using a Delsi Nermag Rock-Eval II system. The method is based on a whole-rock pyrolysis technique that is designed to identify the type and maturity of organic matter and to detect the petroleum potential of the sediments (Tissot and Welte, 1984; Espitalié et al., 1986). The Rock-Eval system involves a temperature program that first releases volatile hydrocarbons (S_1) at 300°C for 3 min. Hydrocarbons are then released by thermal cracking of kerogen (S_2) as the temperature is increased from 300°C to 550°C at 25°C/min. S_1 and S_2 hydrocarbons are measured by a FID. The temperature at which the kerogen releases the maximum amount of S_2 hydrocarbons provides T_{max}, a parameter used to assess the maturity of organic matter. Between 300°C and 390°C of the stepped pyrolysis, CO_2 that was released from the thermal cracking of organic matter (S_3) is trapped and measured by a TCD. For the characterization of organic matter, the following parameters can be calculated: hydrogen index (HI; $100 \times S_2/\text{TOC}$), oxygen index (OI; $100 \times S_3/\text{TOC}$), S_2/S_3 value, and production index (PI; $S_1/(S_1 + S_2)$).

Inorganic Geochemistry

Sampling and Chemical Analyses of Interstitial Water

Shipboard interstitial water analyses were performed on 5- to 35-cm-long whole-round sections that were cut and capped immediately after the core retrieval on deck. In the upper 30 mbsf, two samples per core were collected from cores with sufficient recovery. Below 30 mbsf, one whole-round sample per core was obtained from the bottom of the section with the least apparent drilling disturbance. The sediment was immediately removed from the core liner, and the outer layer, which mostly consists of sediments permeated by drill water (surface seawater), was carefully trimmed to remove any potential contaminants. The cleaned pieces of sediment were placed into a titanium squeezer (modified after Manheim and Sayles, 1974) between two Whatman No. 1 filters that were previously rinsed in high-purity water to remove processing acids. The press was operated up to pressure of about 30,000 psi (205 MPa). The sediment sample remained under pressure until most of the squeezable water was removed. Interstitial water was collected into prewashed 20- to 50-cm^3 plastic syringes and filtered through a disposable 0.45-µm polycarbonate filter. Samples were stored in plastic vials pending shipboard analyses. Aliquots for future shore-based analyses were placed in acid-washed plastic tubes and glass ampoules and heat sealed.

Pore-water samples were routinely analyzed for salinity as total dissolved solids with a Goldberg optical hand-held refractometer (Reichart) and for pH and alkalinity by the Gran titration with a Brinkmann pH electrode and a Metrohm autotitrator. Chloride was analyzed by titration with $AgNO_3$. Calcium and magnesium concentrations were analyzed by ethylene-bis (oxyethyleneitrilo)-tetra-acetic acid (EGTA) and di-sodium-ethylene-tetra acetate (EDTA) acid titration, respectively. Silica, ammonia, and phosphate determinations were carried out by colorimetry using a Milton Roy Spectronic 301 spectrophotometer (Gieskes et al., 1991).

International Association of Physical Sciences Organizations (IAPSO) standard seawater was used for calibrating most techniques. The reproducibility of these analyses, expressed as 1σ standard deviations of means of multiple determinations of IAPSO standard seawater or of a standard, are alkalinity ≤ 1.5%; chloride ≤ 0.3%; calcium ≤ 0.5%; magnesium ≤ 0.5%; silica ≤ 3%; and phosphate and ammonia = 4%. At all sites, sodium was determined using charge-balance calculations where $\sum(\text{cation charge}) = \sum(\text{anion charge})$.

Potassium and sulfate were analyzed by ion chromatography (ICr) using the Dionex DX-100. The reproducibility of these analyses, expressed as 1σ standard deviations of means of multiple determinations of IAPSO standard seawater, are potassium ≈4% and sulfate ≈1%. Potassium was also analyzed by atomic emission spectroscopy (AES), which provides better precision than the ICr, with <2% relative error, and an accuracy of about 0.5% vs. an accuracy of within 5% using the Dionex. Calcium and magnesium were also routinely determined using ICr. For calcium, a precision of ≈5.5% was obtained with ICr as opposed to <0.5% by titration. For magnesium, the precision was within 4% with ICr, and also compared unfavorably with <0.5% relative error by titration. Accuracy of the ICr analyses for Mg and Ca was determined by comparisons to IAPSO standards and was within 5% and 6%, respectively. To obtain some information about the accuracy changes for K, Ca, and Mg as a function of the element concentration ranges in the interstitial water samples, ICr data from Sites 1039 and 1040 were plotted with those obtained from atomic emission and titration methods (Fig. 9). In Table 7, the ICr

data for Mg, Ca, and K are compared with titration data for Mg and Ca and with AES data for K up for Site 1039. The data reported in these figures were corrected for instrumental drift. It appears that ICr data compare favorably with those from the other two methods for samples with element concentrations within or in the range of the interspersed standard used (i.e., 80% IAPSO). However, it seems that the drift correction is useful for Mg for a large range of concentrations up to 20% above and below the standard concentration, whereas it is poor for K to 0.5% below the standard concentration. Ca has an intermediate behavior with a useful drift correction from the 80% IAPSO standard concentration to 12.5 mM (i.e., up to +4 mM, meaning 30% above the standard concentration). Thus, the accuracy of the ICr results could be improved by interspersing standards that have concentrations within the above determined ranges. The problem is how to determine the concentration range of the samples before the ICr Dionex analyses. This can be achieved by spot analyses of a few samples by titration for Ca and Mg and by AES for K, or by a preliminary run of a small subset of samples by ICr. In addition, developing a computer code for drift correction would be an efficient tool for quickly computing the drift calculation. However, the concentration ranges of the calibration curve and interspersed standards must fit closely with those of the samples. Although on this leg the ICr method was not optimized for giving precise and accurate results similar to the titration or atomic emission methods, the ICr results provided a useful check on the general trends of the depth profiles for K, Ca, and Mg.

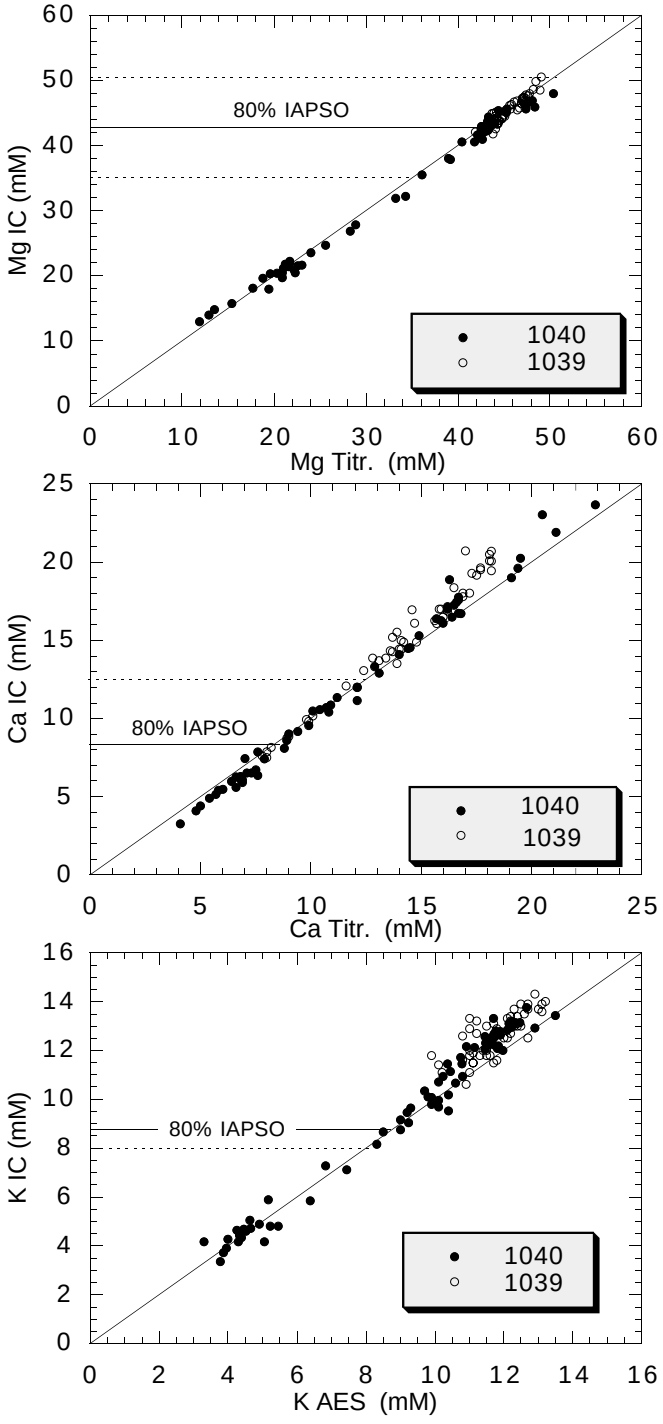

Figure 9. Comparison between ion chromatography and titration methods for Ca and Mg, and between ion chromatography and atomic emission spectroscopy for K. Solid line yields the concentration of the 80% IAPSO interspersed standard that was used. Dashed lines limit concentrations in which the drift correction is useful for Mg, Ca, and K, respectively.

Table 7. Comparison between ion chromatography and titration methods for Mg and Ca concentrations, and with atomic emission spectroscopy for K concentrations of pore fluids of Site 1039.

Core, section, interval (cm)	Depth (mbsf)	Mg (mM)		Ca (mM)		K (mM)	
		ICr	Titr.	ICr	Titr.	ICr	AES
170-1039B-							
1H-1, 145-150	1.45	50.55	49.1	9.93	9.8	13.9	12.7
2H-2, 140-150	4.95	48.52	48.9	8.76	8.9	12.9	11.8
2H-5, 140-150	9.45	49.8	48.5	9.46	8.5	13.0	11.5
3H-2, 140-150	14.45	48.63	48.2	9.28	8.2	13.2	11.2
3H-5, 140-150	18.95	47.78	47.4	8.14	8.2	13.4	12.2
4H-2, 140-150	23.95	47.47	47.2	7.85	8.0	13.7	12.3
4H-5, 140-150	28.45	46.51	47.2	7.6	7.8	13.6	13.1
5H-4, 140-150	36.45	45.76	46.7	7.52	8.0	13.1	11.7
6H-4, 140-150	45.93	45.62	45.7	10.17	8.6	13.4	12.4
7H-4, 140-150	55.45	45.12	45.2	8.83	9.0	13.7	12.7
8H-4, 140-150	64.95	44.47	45.1	9.82	9.9	13.0	12.3
9H-4, 140-150	74.45	43.43	43.2	10.15	10.1	13.0	12.5
10H-4, 140-150	83.95	43.55	43.4	12.08	11.6	13.3	12.1
11H-5, 140-150	94.95	42.84	40.0	13.07	12.4	13.0	12.4
12X-3, 135-150	101.43	42.77	42.8	13.86	12.8	13.0	12.4
13X-6, 135-150	112.43	42.07	41.9	13.69	13.1	14.0	13.2
14X-3, 135-150	117.53	41.93	42.5	13.85	13.4	13.7	13.0
15X-6, 135-150	131.63	42.81	43.1	14.44	14.1	13.9	13.1
16X-3, 135-150	136.63	42.28	43.1	14.98	14.1	13.5	12.6
17X-4, 135-150	147.73	41.78	43.8	14.88	14.2	13.9	12.5
18X-4, 135-150	157.33	42.52	44.1	22.86	14.3	14.3	12.9
19X-5, 135-150	168.53	43.24	44.3	16.96	14.6	13.1	12.4
20X-5, 135-150	178.03	43.38	44.3	17	15.9	13.2	12.2
21X-5, 135-150	187.63	43.49	44.4	16.27	15.6	12.5	12.7
22X-5, 135-150	197.23	44.52	44.1	18.37	16.5	12.0	11.0
23X-5, 135-150	206.93	44.22	44.2	18.03	16.9	11.5	11.1
24X-5, 135-150	216.53	43.89	44.4	17.81	16.9	11.8	11.3
25X-5, 135-150	226.13	43.83	44.5	18.01	17.2	11.8	11.5
26X-4, 135-150	232.83	44.9	43.7	19.51	17.7	11.8	11.0
27X-5, 135-150	245.43	45.01	43.9	20.09	18.1	11.5	11.1
28X-3, 135-150	252.13	44.68	45.0	20.49	18.1	11.4	10.1
29X-3, 135-150	261.83	44.06	44.8	19.45	18.2	11.6	10.8
30X-2, 135-150	270.03	45.21	45.2	24.83	18.6	10.6	10.9
31X-2, 130-150	279.60	45.15	44.2	20.69	18.2	11.1	11.0
32X-2, 130-150	289.30	44.23	44.8	19.64	17.7	11.6	11.8
33X-3, 130-150	300.40	45.41	45.2	20.07	18.2	12.0	11.5
34X-3, 130-150	309.90	46.14	45.6	19.16	17.5	11.9	11.1
35X-3, 130-150	319.60	46.27	45.8	19.3	17.3	11.8	9.90
36X-5, 130-150	332.20	46.66	46.1	20.74	17.0	12.6	10.8
37X-5, 130-150	341.80	45.43	46.5	16.86	16.2	12.1	11.5
38X-3, 130-150	348.40	46.23	47.3	17.01	15.8	12.2	11.5
39X-5, 130-150	361.00	46.48	46.9	16.09	14.7	12.7	11.2
40X-6, 130-150	372.10	47.39	47.2	15.2	13.7	13.3	11.0
41X-1, 130-150	374.20	47.99	47.8	15.51	13.9	12.9	11
170-1039C-							
1R-2, 125-150	1.45	46.66	47.1	16.49	16.0	11.5	11.7
2R-1, 65-100	4.95	47.11	47.1	16.08	15.7	12	11.4
3R-2, 132-150	9.45	46.86	46.4	14.89	14.8	12.7	12.2
4R-1, 132-150	14.45	46.92	47.1	14.27	13.7	12.5	12.0
5R-1, 0-6	18.95	46.79	47.7	13.52	13.9	12.5	12.1
6R-4, 128-142	23.95	47.61	47.6	14.34	13.6	11.8	11.6
7R-1, 85-100	28.45	47.26	47.0	14.44	14.0	11.1	10.2

Note: ICr = ion chromatography, Titr. = titration, and AES = atomic emission spectroscopy.

Sampling of the Bottom Seawater

During Leg 170, the water-sampling temperature probe (WSTP) tool (Barnes, 1988) was used for sampling bottom seawater at each drilling site. The tool was lowered on the coring wire to the end of the drill string, where it hooks onto an assembly just above the bit. The bit was lowered into bottom water, ~50 m above mudline, without pumping to avoid mixing surface seawater (drill water) with bottom seawater. A time-operated valve opens and water is drawn under negative pressure through the filter and into the WSTP. After passing through the filter assembly, the fluid enters the sample reservoir via 1/16-in titanium tubing, connected to a titanium sample coil. A one-way valve is connected to the other end of the coil, which allows fluid to pass into a stainless-steel overflow cylinder.

Before deployment, the fluid path is backfilled with distilled water that has been previously degassed by nitrogen bubbling. The overflow cylinder is flushed with nitrogen and evacuated. A timer is set for a fixed time after which the valve opens, exposing the sampling line and chamber to ambient pressure. The timer also closes the valve after a prearranged time interval; 5 min was used on this leg. Subsequently, a bottom-water temperature was also obtained.

Fluid from the titanium and stainless-steel coils was filtered (0.45 µm) and analyzed following the procedures described for the interstitial water squeezed from whole-round samples. Chemical data for interstitial waters and bottom seawaters are reported in molar units.

X-ray Fluorescence Analysis

Major and trace element analyses were carried out on igneous rocks and siliciclastic and calcareous sediments using the methods described in the Leg 139 *Initial Reports* volume (Shipboard Scientific Party, 1992a). Operating conditions for the fully automated wavelength dispersive ARL 8420 XRF are given in Table 8. Major element samples for Leg 170 were prepared using either the Claisse fluxer or the NT-2100 bead sampler. Major element analyses for the diabase Standard BAS-140, prepared using both the Claisse fluxer and the bead sampler, are reported in Table 9, showing the good agreement between the two methods. In the absence of an automated agate mortar and pestle, samples were ground using the SPEX 8510 shatterbox with a tungsten carbide barrel, resulting in significant W contamination and minor Ta, Co, and Nb contamination.

The sediments were measured against a calibration prepared using 23 standards to cover the wide range of major and trace element compositions expected for the sediments. Major and trace element compositions were determined 23 times for sediment Standard SCo-1 over the course of the cruise, to establish external reproducibility and accuracy at concentration levels typical of those measured in the Leg 170 sediments. The data are compiled in Tables 10 and 11. The major element data are both precise and accurate to within 2%, except for Na_2O and P_2O_5, which are accurate and precise to 25%–30%. Trace elements are also accurate and precise to within 2%–3%, except for Nb, which is within 10%.

The gabbroic and basaltic rocks were analyzed against a basalt calibration using eight basaltic and gabbroic standards. Six replicate analyses of BIR-1 were measured during the cruise to evaluate external reproducibility, and the data are compiled in Tables 10 and 11. The major element data at basaltic concentration levels are precise within 1%–2% except for MnO and P_2O_5, which are precise within 5%–10%, and K_2O, which varies by ~30% at these low concentrations. Trace element concentrations for BIR-1 are generally lower than those measured in Leg 170 gabbroic and basaltic rocks. For BIR-1, Nb, Rb, Ce, and Ba are near or below detection limits. Other trace elements are generally precise to within 2%–3%.

PHYSICAL PROPERTIES

General Objectives

The principal objectives of the physical properties measurement program are closely connected to the main scientific and operational goals of this cruise. These objectives can be grouped together as follows:

1. Provide comprehensive physical properties data sets, including porosity and mechanical and acoustic variations.
2. Integrate core physical properties data with physical parameters derived from downhole measurements, including LWD, APC temperature tool, WSTP, and DVTP.

Table 8. X-ray fluorescence operating conditions and detection limits for Leg 170.

Oxide or element	Line	Crystal	Detector	Collimator	Peak angle (°2θ)	Background offset (°2θ)	Count time on peak (s)	Count time on background (s)	Detection limit
SiO_2	Kα	PET	FPC	Medium	109.21		100		0.03%
TiO_2	Kα	LIF200	FPC	Fine	86.14		100		0.01%
Al_2O_3	Kα	PET	FPC	Medium	145.12		100		0.01%
Fe_2O_3	Kα	LIF200	FPC	Fine	57.52		40		0.01%
MnO	Kα	LIF200	FPC	Fine	62.97		100		0.005%
MgO	Kα	TLAP	FPC	Medium	45.17	±0.80	150	150	0.05%
CaO	Kα	LIF200	FPC	Medium	113.09		40		0.005%
Na_2O	Kα	TLAP	FPC	Medium	55.10	–1.20	150	150	0.1%
K_2O	Kα	LIF200	FPC	Medium	136.69		100		0.005%
P_2O_5	Kα	GE111	FPC	Medium	141.04		100		0.005%
Rh	Kα-C	LIF200	Scint	Fine	18.56		100		
Nb	Kα	LIF200	Scint	Fine	21.40	+0.30	200	200	1 ppm
Zr	Kα	LIF200	Scint	Fine	22.55	–0.35	100	100	1 ppm
Y	Kα	LIF200	Scint	Fine	23.80	–0.30	100	100	1 ppm
Sr	Kα	LIF200	Scint	Fine	25.15	–0.35	100	100	1 ppm
Rb	Kα	LIF200	Scint	Fine	26.62	+0.40	100	100	1 ppm
Zn	Kα	LIF200	Scint	Fine	41.81	+0.40	100	100	2 ppm
Cu	Kα	LIF200	Scint	Fine	45.03	–0.40	100	100	2 ppm
Ni	Kα	LIF200	Scint	Fine	48.67	–0.40	100	100	2 ppm
Cr	Kα	LIF200	FPC	Fine	69.35	–0.50	100	100	3 ppm
Fe	Kα	LIF220	FPC	Fine	85.64	+0.80	100	100	
V	Kα	LIF220	FPC	Fine	123.06	–0.50	100	100	4 ppm
Ti	Kα	LIF200	FPC	Fine	86.14	–0.50	100	100	
Ce	Lα	LIF220	FPC	Medium	128.16	+1.89	100	100	10 ppm
Ba	Lβ	LIF220	FPC	Medium	128.78	+1.31	100	100	15 ppm

Notes: Analyses were performed using a rhodium-target X-ray tube operated at 30 kV and 80 mA for major elements, 50 kV and 50 mA for trace elements. Detectors: FPC = flow proportional counter (P_{10} gas), Scint = NaI scintillation counter. Elements Rh, Fe, and Ti were measured by the trace element program for matrix and interference corrections only.

Table 9. Comparison of major element results using Claisse fluxer and the NT-2100 Bead Sampler.

			SiO_2	TiO_2	Al_2O_3	Fe_2O_3	MnO	MgO	CaO	Na_2O	K_2O	P_2O_5	Total
BAS-140†		Published value	50.50	0.98	14.60	11.10	0.19	8.15	12.40	1.84	0.01	0.08	99.85
Diabase	A	7-Nov-96 5:47	51.15	1.04	14.98	11.44	0.19	8.24	12.63	1.10	0.03	0.039	100.84
	B	7-Nov-96 6:15	51.12	1.04	14.93	11.38	0.19	8.19	12.60	1.07	0.03	0.038	100.58
		Difference	0.03	0.00	0.05	0.06	0.00	0.05	0.03	0.03	0.00	0.00	0.25
		% difference A/B	0.06	0.00	0.33	0.52	0.53	0.61	0.24	2.73	3.70	2.56	0.25
	A	% diff. pub. value	1.29	6.12	2.60	3.06	0.00	1.10	1.85	–40.22	170.00	–51.25	0.99
	B	% diff. pub. value	1.21	5.77	2.21	2.46	–0.53	0.49	1.59	–71.96	61.54	–110.53	0.73
BAS-140*		Published value	50.50	0.98	14.60	11.10	0.19	8.15	12.40	1.84	0.01	0.08	99.85
Diabase	A	28-Oct-96 9:54	50.51	1.00	14.54	11.30	0.19	8.01	12.42	1.91	0.02	0.07	99.97
	B	27-Oct-96 17:17	50.69	0.95	14.53	11.20	0.19	8.13	12.53	1.91	0.02	0.07	100.22
		Difference	0.18	–0.05	–0.01	–0.10	0.00	0.12	0.11	0.00	0.00	0.00	0.25
		% difference A/B	0.36	–5.26	–0.07	–0.89	0.00	1.48	0.88	0.00	0.00	0.00	0.25
	A	% diff. pub. value	0.38	–3.06	–0.48	0.90	0.00	–0.25	1.05	3.80	100.00	–12.50	0.37
	B	% diff. pub. value	0.02	2.00	–0.41	1.77	0.00	–1.75	0.16	3.66	50.00	–14.29	0.12
BAS-140‡		Published value	50.50	0.98	14.60	11.10	0.19	8.15	12.40	1.84	0.01	0.08	99.85
Diabase	A	10-Nov-96 6:21	51.23	0.94	14.55	11.57	0.19	8.06	12.60	1.96	0.02	0.07	101.19
	B	10-Nov-96 6:48	51.84	0.99	14.80	11.81	0.20	8.18	12.74	1.89	0.02	0.07	102.54
		Difference	–0.61	–0.05	–0.25	–0.24	–0.01	–0.12	–0.14	0.07	0.00	0.00	–1.35
		% difference A/B	–1.19	–5.32	–1.72	–2.07	–5.26	–1.49	–1.11	3.57	0.00	0.00	–1.33
	A	% diff. pub. value	1.45	–4.08	–0.34	4.23	0.00	–1.10	1.61	6.52	100.00	–12.50	1.34
	B	% diff. pub. value	2.58	1.01	1.35	6.01	5.00	0.37	2.67	2.65	50.00	–14.29	2.62
BAS-140**		Published value	50.50	0.98	14.60	11.10	0.19	8.15	12.40	1.84	0.01	0.08	99.85
Diabase	A	10-Nov-96 7:44	50.20	0.99	14.65	11.31	0.19	8.02	12.40	1.08	0.03	0.04	98.91
	B	10-Nov-96 0:00	50.39	1.01	14.72	11.37	0.19	8.09	12.46	1.13	0.03	0.04	99.43
		Difference	–0.19	–0.02	–0.07	–0.06	0.00	–0.07	–0.06	–0.05	0.00	0.00	–0.52
		% difference A/B	–0.38	–2.02	–0.48	–0.53	1.04	–0.87	–0.48	–4.63	–7.69	0.00	–0.53
	A	% diff. pub. value	–0.59	1.02	0.34	1.89	1.05	–1.60	0.00	–41.30	160.00	–48.75	–0.94
	B	% diff. pub. value	–0.22	2.97	0.82	2.37	0.00	–0.74	0.48	–62.83	64.29	–95.12	–0.42

Note: All analyzing conditions during the Leg 170 calibration are the same as those during the Leg 169 calibration with the exception of the collimator on TiO_2. † = beads made with Flux V using Claisse (Leg 170) run during Leg 169 calibration (MAJX). Standard weighed at Site 1040 - Flux V weighed onshore. * = beads made with Flux VII using Bead Sampler (Leg 170) run during Leg 170 calibration. Standard and flux VII weighed on board during Leg 170 transit (see cell note). ‡ = beads made with Flux VII using Claisse (Leg 170) run during Leg 170 calibration. Standard weighed on board during Leg 170 at Site 1039. ** = beads made with Flux VII using Claisse (Leg 170) run during Leg 169 calibration (MAJX). Standard weighed on board during Leg 170 at Site 1039.

Table 10. Replicate major element analyses of SCo-1 and BIR-1 during Leg 170.

	SiO_2	TiO_2	Al_2O_3	Fe_2O_3	MnO	MgO	CaO	Na_2O	K_2O	P_2O_5	Total
SCo-1 (A)											
Accepted:	68.8	0.69	14.98	5.63	0.060	2.98	2.87	0.99	3.040	0.230	100.27
Measured:	68.45	0.72	15.24	5.70	0.049	3.19	2.80	0.56	3.010	0.200	99.92
	68.37	0.70	15.33	5.64	0.053	3.11	2.82	0.67	2.999	0.199	99.89
	68.09	0.69	15.27	5.70	0.056	3.09	2.81	0.71	3.005	0.199	99.62
	68.44	0.69	15.38	5.69	0.056	3.10	2.84	0.70	3.012	0.201	100.11
	68.73	0.73	15.33	5.84	0.051	3.15	2.84	0.65	3.031	0.203	100.56
	68.27	0.71	15.21	5.72	0.055	3.13	2.82	0.60	3.016	0.199	99.73
	68.24	0.70	15.17	5.70	0.054	3.12	2.82	0.70	3.011	0.198	99.71
	68.55	0.71	15.29	5.72	0.057	3.16	2.84	0.63	3.024	0.200	100.18
	68.6	0.70	15.23	5.69	0.056	3.17	2.84	0.57	3.009	0.200	100.08
	68.6	0.70	15.23	5.69	0.056	3.17	2.84	0.57	3.009	0.200	100.08
	68.93	0.72	15.26	5.78	0.057	3.16	2.84	0.55	3.027	0.200	100.52
	68.95	0.71	15.26	5.72	0.054	3.18	2.85	0.63	3.024	0.202	100.58
	68.63	0.70	15.19	5.68	0.051	3.17	2.84	0.67	3.007	0.202	100.14
	68.74	0.69	15.18	5.70	0.058	3.14	2.83	0.62	3.008	0.202	100.17
	68.74	0.69	15.18	5.70	0.058	3.14	2.83	0.62	3.008	0.202	100.17
	69.10	0.72	15.31	5.75	0.058	3.25	2.84	0.51	3.024	0.203	100.77
	68.91	0.70	15.30	5.75	0.057	3.10	2.83	0.62	3.010	0.203	100.48
	68.66	0.70	15.27	5.72	0.057	3.13	2.84	0.62	3.011	0.202	100.21
	68.38	0.66	14.88	5.61	0.057	2.91	2.78	1.05	2.972	0.219	99.52
	68.70	0.71	15.38	5.62	0.059	3.08	2.87	0.80	3.041	0.221	100.48
	68.69	0.72	15.33	5.72	0.056	3.12	2.87	0.85	3.038	0.224	100.62
	68.78	0.73	15.47	5.58	0.051	3.27	2.87	0.67	3.047	0.223	100.69
	68.68	0.72	15.13	5.62	0.054	3.16	2.89	0.81	3.051	0.225	100.34
	68.50	0.69	15.12	5.57	0.053	3.07	2.88	0.98	3.033	0.225	100.12
	68.48	0.71	15.45	5.67	0.056	3.14	2.86	0.85	3.032	0.226	100.47
	68.48	0.71	15.45	5.67	0.056	3.14	2.86	0.85	3.032	0.226	100.47
BIR-1											
Accepted:	47.42	0.95	15.35	11.34	0.17	9.52	13.21	1.81	0.02	0.02	99.82
Measured:	47.06	0.92	15.31	11.26	0.179	9.36	13.12	1.85	0.032	0.024	99.12
	47.62	0.93	15.43	11.39	0.178	9.52	13.21	1.86	0.031	0.026	100.20
	47.50	0.95	15.36	11.22	0.177	9.52	13.17	1.75	0.036	0.025	99.71
	47.32	0.89	15.30	11.32	0.175	9.42	13.16	1.93	0.028	0.025	99.57
	47.6	0.92	15.42	11.33	0.178	9.52	13.16	1.92	0.031	0.025	100.1
	47.96	0.98	15.50	11.39	0.178	9.65	13.28	1.82	0.038	0.025	100.82
	47.74	0.95	15.41	11.28	0.177	9.63	13.19	1.93	0.035	0.024	100.37
	47.47	0.99	15.40	11.38	0.177	9.70	13.15	1.73	0.039	0.025	100.06
	47.71	1.00	15.55	11.45	0.178	9.74	13.24	1.65	0.040	0.026	100.58

Note: All concentrations are in wt%.

Table 11. Replicate trace element analyses of SCo-1 and BIR-1 during Leg 170.

	Nb	Zr	Y	Sr	Rb	Zn	Cu	Ni	Cr	V	Ce	Ba
SCo-1												
Accepted:	12	174	23	166	112	103	29	26	68	131	58	570
Measured:	10.5	181.2	22.3	164.3	114.4	104	30	26	71	144	55	557
	10.9	179.9	23.5	165.2	115.7	105	30	26	72	141	58	552
	12.4	175.2	21.4	165.7	116.6	107	31	27	70	135	51	559
	12.7	178.1	20.6	165.3	115.6	104	30	28	70	139	46	573
	10.3	176.4	22.5	164.3	113.7	103	28	26	70	139	61	559
	11.6	176.9	21.9	165.0	114.2	105	29	27	69	139	55	558
	12.7	178.9	21.3	164.0	117.0	105	31	29	68	136	52	570
	12.3	176.0	20.6	163.9	116.8	105	30	28	71	138	51	563
	11.7	181.5	21.5	165.6	114.6	104	30	27	71	135	55	555
	10.9	174.3	21.1	163.9	114.0	104	29	26	71	143	54	566
	12.7	177.2	22.7	165.2	115.6	105	28	28	69	137	48	566
	12.8	178.7	21.5	165.4	116.1	104	28	28	69	139	58	560
	12.5	177.0	21.7	165.3	116.5	104	29	28	69	144	58	553
	11.3	179.1	20.8	163.5	114.3	103	30	28	71	139	52	573
	11.7	176.4	21.6	164.7	113.7	103	30	27	72	138	56	564
	11.9	174.9	22.3	164.5	115.5	104	27	27	69	142	54	566
	12.1	180.2	21.6	165.5	116.0	104	30	28	70	138	51	576
	10.2	179.1	21.6	162.6	115.3	105	30	27	71	141	50	560
	11.0	179.0	21.7	162.9	113.9	104	29	28	69	140	54	565
	11.0	180.6	21.3	163.3	114.6	105	28	27	67	140	51	580
	11.6	179.1	22.3	163.3	115.3	104	29	26	68	140	55	555
	12.8	177.7	20.8	163.4	115.4	107	30	28	70	140	53	556
	12.1	176.7	21.4	165.3	116.1	105	31	27	70	144	51	555
BIR-1												
Accepted:	0.5	14	15.5	108	0.4	71	126	163	379	310	2.5	6.8
Measured:	0.7	11.5	14.2	110.4	1.1	73	134	162	381	291	0	15
	1.2	12.9	15.7	109.6	0.8	72	130	161	383	303	1	1
	–0.8	13.0	15.8	109.0	–0.3	72	130	160	388	307	0	–1
	–0.3	13.1	14.8	109.5	0.6	73	128	163	391	302	6	2
	0.6	13.0	15.6	110.3	0.7	72	131	162	385	304	6	–10

Note: All concentrations are in ppm.

3. Provide an initial assessment of physical and deformational properties of sediment during accretion.
4. Correlate between holes at the seaward reference Site 1039, where cores were sampled extensively for paleoceanographic purposes by the sedimentologic, paleontologic, geochemical, and magnetostratigraphic groups.

Physical properties were measured on whole-round cores and on the undisturbed parts of split cores. The multisensor track (MST) was used for nondestructive, whole-round core measurements of wet bulk density, *P*-wave velocity, natural gamma radiation, and magnetic susceptibility. Needle probe thermal conductivity measurements were conducted on whole-round cores. Undrained shear strength, unconfined compressive strength, electrical resistivity, and *P*-wave velocity were measured on split sections. Parts of split cores that were undisturbed by drilling and sampling, gas expansion, bioturbation, cracking, pocking, and large voids were selected for sample collection to obtain laboratory-measured properties (wet bulk density, grain density, dry bulk density, water content, void ratio, and porosity). A moderate number of whole-round samples from APC/XCB-cored sections was taken for shore-based laboratory measurements of consolidation, permeability, triaxial testing, and X-ray tomography.

Sampling Strategy

To accommodate these general objectives, the sampling program for physical properties was planned to fulfill several requirements. Whole-core sections were scanned with the MST before being split. Physical properties samples were then selected from the split cores. Where recovery permitted, one or two samples per section were chosen to represent the dominant lithology. Core specimens for analyses were selected in conjunction with sedimentologists and structural geologists. Additional samples were selected to represent intervals of unusual lithology or structure. Freeze-dried samples from the moisture and density sample were forwarded to the chemistry laboratory for carbonate analyses, and splits from the dried portion of these samples were used for bulk XRD mineralogical determinations and total carbon measurements. Two samples per core were selected for shore-based XRD and grain-size analysis to provide constraints on clay content. Samples for shore-based chemical studies were also analyzed by the shipboard physical properties group.

Multisensor Track

The MST included four physical properties sensors: the magnetic susceptibility logger (MSL), the gamma-ray attenuation (GRA), the *P*-wave logger (PWL), and the natural gamma radiation (NGR) detector. (The NGR was operational only for Sites 1041, 1042, and 1043). Individual, unsplit core sections were placed on the MST, which automatically moved the section through the sensors on a fiberglass track.

MST data were sampled at discrete intervals, with the sampling rate chosen to optimize the resolution of the data and the time necessary to run each core section through the device. GRA, PWL, and MSL were set to measure at an interval of 2 cm and at acquisition times of 5 s. Guidance for the selection of the sampling interval based on the size of the instrument sensing region was obtained from Boyce (1973, 1976) for GRA, Schultheiss and McPhail (1989) for PWL, and Hoppie et al. (1994) for NGR.

Magnetic susceptibility was measured on all sections using the lower sensitivity, 1.0 range on the Bartington Model MS2 meter with an 8-cm-diameter loop; the meter was set to record in SI units, but no correction was applied for the difference in loop and core diameter or the diamagnetic effect of the core conveyor and core liner. The values are therefore relative volume susceptibility values. The close sampling interval for magnetic susceptibility was chosen to increase the possibility of correlating data between holes and to provide a high-resolution data set for paleomagnetic studies.

GRA-density measurements were made by comparing the gamma-ray attenuation of the sediment with the degree of attenuation through water-surrounded standards of aluminum cylinders of different thicknesses. Aluminum cylinders used as calibration standards

were 0, 2, 3, 4, and 5 cm in diameter, for which the average water + aluminum densities were 1.024, 1.534, 1.790, 2.046, and 2.301 g/cm^3, respectively. The GRA device was calibrated approximately every 15–20 sections, or 3–4 times per day at most, using an acquisition time of 30 s.

P-wave Measurements

P-wave velocities were measured both with the PWL mounted on the MST and with transducers on the split-core track. The PWL measured *P*-wave velocity at a high sampling density orthogonal to the long axis of whole-round core sections. The split-core track was used to measure *P*-wave velocity at discrete locations.

The velocity calculation is based on the traveltime of an acoustic impulse signal transmitted between two piezoelectric transducers inserted in the split sediment cores. The transmitted signal used on the split-core measurements is a 0.1-µs square wave with a period of 0.2 ms. The return signal is stored by the computer. For the split-core measurements, the automatic picking routine generally selected noise near the beginning of the digitizing window, which required hand picking the first arrival. The system software automatically calculates sediment velocity.

The PWL transmits 500-kHz *P*-wave pulses through the core at a rate of five measurements per second. The transmitting and receiving transducers are aligned perpendicular to the core axis, while a pair of displacement transducers monitored the separation between them. For the plastic core liner, a nominal thickness of 2.64 mm and a liner velocity of 1987 m/s were used. Accurate velocities with the PWL could be determined for APC cores. However, accurate velocities were obtained for XCB cores where the core completely filled the liner (such as in the carbonate section).

The PWL was calibrated several times per site using four blocks of acrylic standards of different length. The system automatically performed a regression of transducer separation vs. traveltime; a typical velocity was 2732 m/s with an intercept (or delay time) of 2.0808 µs.

P-wave velocity was measured on split-core sections using transducers on the split-core track. The sampling interval was usually two per section. The PWS1 transducer pair has a fixed separation of 7.0 cm and, in soft sediment, is inserted along the axis of the core to measure velocity parallel to core length, which is commonly orthogonal to bedding. The PWS2 transducer (separation of 3.5 cm) measures velocity roughly parallel to bedding and is inserted perpendicular to the core's axis. Readings of a digital thermometer inserted into the sample were also logged. The transducer calibration was checked using a split-core liner segment filled with distilled water. The PWS1 and PWS2 transducers were used only in the upper 50 m at most sites (e.g. Site 1039), because induration of the sediment did not permit insertion of the transducers without disturbing or cracking the sediment.

Where core material became too consolidated to insert the PWS1 or PWS2 transducers, velocity measurements were made using contact transducers (PWS3) at a signal frequency of 500 kHz. Sample thickness was measured automatically by a digital gauge. Seawater was used to improve the acoustic coupling between the sample and the transducers. Most PWS3 measurements were performed on the split cores through the core liner. On some cores, drilling mud separated the core and the core liner. For these cores, discrete samples were cut for direct insertion between the transducers. In a manner similar to that described for PWL calibration, PWS3 calibration was checked using a series of polycarbon standards.

Moisture and Density (MAD) Measurements

Water content, wet bulk density, dry bulk density, grain density, and porosity were routinely determined using 10-cm^3 specimens collected from split cores. Immediately after collection of the samples, wet sediment mass (M_t) was measured. Dry sediment mass (M_d) and dry sediment volume (V_d) were determined after the samples had dried for 24 hr at a temperature of 105° ± 5°C.

Wet and dry sample mass were determined to a precision of ±0.01 g using a Scientech electronic balance. The sample mass was calculated using the acceleration determined on a reference balance with a known mass. The Quantachrome pycnometer was used to determine sample volume to an approximate precision of ±0.02 cm^3. Volume determination is based on the helium-displacement principle (see ASTM D854 Standard [ASTM, 1992]). A reference volume was run periodically (at least once every few cores) in each chamber to check for systematic error, and calibrations, if needed, were performed if errors were greater than the desired precision.

Calculations

The measurement of sample mass and volume was coordinated by the MAD interactive software system, which had been implemented in production mode just before Leg 170. The mass of glass sample-holding beakers was measured at the start of the leg. Beaker volumes were calculated from an assumed density for the beaker material (Pyrex). The density of Pyrex, determined by grinding six beakers and measuring their mass and volume, was found to be 2.22 g/cm^3.

Calculations of phase relations were performed on an Excel spreadsheet that was created during the leg to provide these values. Calculations followed ODP Method C, utilizing the dry volume of sediment and back-calculating for the wet sample volume (e.g., Shipboard Scientific Party, 1996a, 1996b). Calculations include a correction for the residual pore-water salt left behind by drying; the salt mass was determined from the amount of water evaporated, using an assumed salinity of 35, and the salt volume was calculated from a salt density of 2.068 g/cm^3, as determined during the leg. Results of the seawater drying experiment are summarized in Table 12.

Sediment Drying Techniques: Oven and Freeze Drying

Determination of porosity, water content, bulk density, and grain density of a sediment sample depends upon an accurate measurement of its moisture-free and water-saturated mass and volume. Drying of discrete sediment samples, commonly 8- to 10-g specimens placed in small (10 cm^3) glass beakers, is routinely carried out by oven heating for at least 24 hr at a temperature of 105°C. However, concerns exist that oven heating also drives off interlayered water from clay minerals, in particular smectite (Brown and Ransom, 1996). Oven heating thus results in a weight-loss based calculation of interstitial porosity that is higher than exists in situ.

An alternative method of drying discrete sediment samples is freeze drying, although the low humidity involved in this water-removing technique may also extract interlayered water (Brown and Ransom, 1996). An experiment was run to determine whether similar or different porosity values resulted from oven and freeze drying of closely adjacent (1–2 cm) samples of sediment recovered at Sites 1039, 1040, and 1043. Site 1039 cores chiefly contained oceanic pe-

Table 12. Measured mass and volume used to determine density of sea salt, evaporated from a quantity of seawater during Leg 170.

Mass (g)	Volume (cm^3)	Density (g/cm^3)	Standard deviation (g/cm^3)
12.928	6.208	2.082	0.007
10.053	4.877	2.061	0.011
12.246	5.952	2.058	0.008
11.813	5.702	2.072	0.007
11.494	5.565	2.065	0.006

Note: The average salt density is 2.068 (±0.008) g/cm^3.

lagic and hemipelagic deposits of clayey diatom ooze and chalk of relatively high porosity (65%–75%). Sediment that was cored at Site 1040 is a combination of a sequence of terrigenous clayey silt and silty clay of relatively low porosity (40%–60%) overlying the same stratigraphic section that was cored at Site 1039, but compressed to a average porosity of about 60%. Drying-time experiments were run to ensure that the duration of oven and freeze drying was sufficient to drive off all releasable water. The drying time curves for both freeze-dried and oven-dried samples were similar, generally requiring at least 15–20 hr to reach mass stability (<± 0.1 g).

For Site 1039 and 1040 cores, porosity data were gathered on 137 pairs of sediment samples, 85% (117) of which record an oven-dried porosity value exceeding that of the companion freeze-dried sample. Figure 10 displays statistical details of experimental results. The mean porosity of oven-dried samples is 1.9% greater than that of freeze-dried samples (67.1% vs. 65.2%, respectively).

To determine if the difference might be related to contrasting drying techniques, artificial sediment samples of glass beads (coarse sand in size) and seawater were prepared, and three identical sample pairs were oven and freeze dried. The corresponding average porosity and grain density values of oven- and freeze-dried pairs were, respectively, 42.8% and 43.0%, and 2.51 and 2.51 g/cm^3. These effectively matching measurements imply that the higher oven-dried porosity values of Sites 1039 and 1040 sediment can be linked to the lithologic composition of the sediment rather than to the desiccation effectiveness with respect to pore-fluids of shipboard oven- and freeze-drying procedures. Most likely, as noted by Brown and Ransom (1996), the difference is tied to the presence of clay minerals, most likely smectite, and possible also ash layers, than any contrast in the ability of shipboard oven- and freeze-drying experimental equipment to extract interlayered water. This supposition can be further tested by post-cruise analyses of the clay-mineral and ash composition of samples from Sites 1039, 1040, and 1043. A full report on the oven- and freeze-drying experiment is included in the Appendix to the "Explanatory Notes" chapter on CD-ROM (back pocket, this volume).

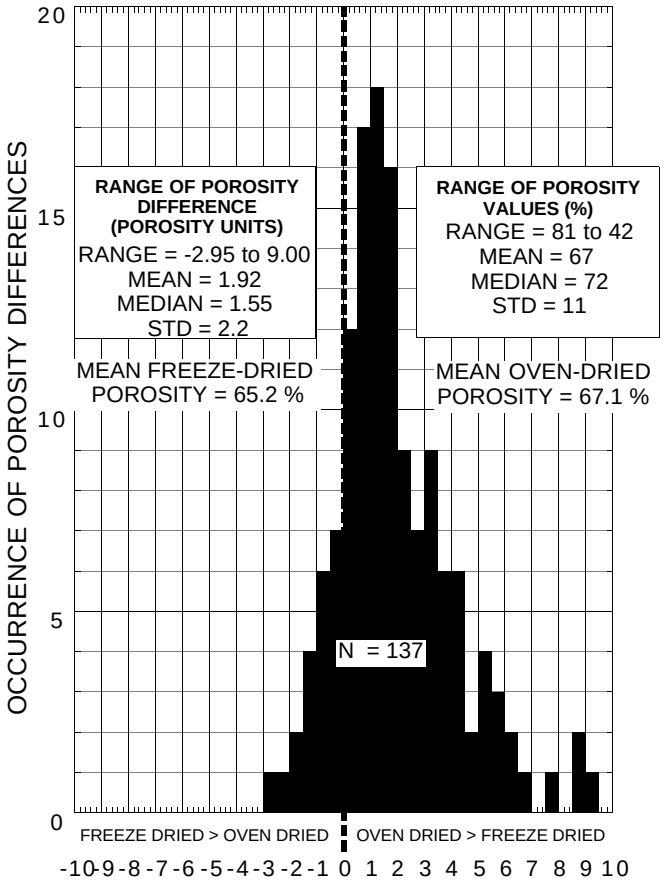

Figure 10. Difference in oven- and freeze-dried porosity values for adjacent sediment samples (Sites 1039 and 1040).

Thermal Conductivity

Thermal conductivity data were routinely collected at two locations per core, and at three or four locations when time permitted. The primary method was the "full space" needle probe technique of von Herzen and Maxwell (1959). Apparent sediment thermal conductivity adjacent to a given needle probe is approximately proportional to the ratio of temperature and the natural logarithm of time once a linear correction for drift has been included. No corrections for temperature or pressure conditions were made as part of the thermal conductivity collection procedure (Ratcliffe, 1960).

Collection of thermal conductivity data was controlled by a preprogrammed microprocessor, the Thermcon-85. Prior to data collection, a drift survey measured temperature changes for a minimum of 120 s. Thermal conductivity data collection proceeded only when drift no longer exceeded 0.04°C/min for any of the needle probes. During the data collection phase, the microprocessor applied constant heat to each needle for 6 min. Reference voltage, the resistance measured by each of the probes, and the current were sequentially logged by the Thermcon unit. A dedicated PC computer attached to the Thermcon unit stored the data.

To determine thermal conductivity, the measured resistances were first converted into temperatures using calibration constants and drift corrections for each needle. Each probe was calibrated by conducting measurements on four standards of known thermal conductivity. The standards used were black rubber, gelatin, red rubber, and macor ceramic, with known thermal conductivities of, respectively, 0.54, 0.67, 0.96 and 1.61 W/(m·K). A linear regression of known thermal conductivity, k_{corr}, to probe reading, k_{meas}, indicates a correction given by $k_{corr} = a + b \times k_{meas}$. Measured and known conductivities for each probe are displayed in Figure 11A, with original data given in Table 13.

Cores were first passively equilibrated to near room temperature (nominally to 21°C) for at least 3 hr. The needle probes were then inserted into the core through holes drilled in the liner. Care was taken to avoid insertion of the needle probes into visible voids or into liquid parts of the core.

All five thermal conductivity needles were used simultaneously whenever possible. On many runs, four needles measured thermal conductivity in the cores, and one needle was placed in a black rubber standard. Each of the five available needles was systematically rotated through different holes in the standard during sequential runs. Most thermal conductivity determinations were made using data collected between 60 and 240 s from the beginning of the heating interval. Errors typically ranged between 5% and 10%.

On lithified or hard-rock samples, thermal conductivity was measured using the "half-space" method of Vacquier (1985), controlled by the TK04 high-precision thermal conductivity meter. The needle probe was sandwiched between the flat surface of a split-core sample and that of an epoxy block. All half-space measurements were conducted in a seawater bath equilibrated to room temperature to keep the samples saturated, to improve thermal contact between the needle and the sample, and to reduce thermal drift during the tests. Results of control measurements are given in Figure 11B and Table 14.

In Situ Temperature Measurements and Bottom-Water Sampling

In situ thermal measurements were made using the APC temperature shoe, the thermal capability of the water-sampling temperature

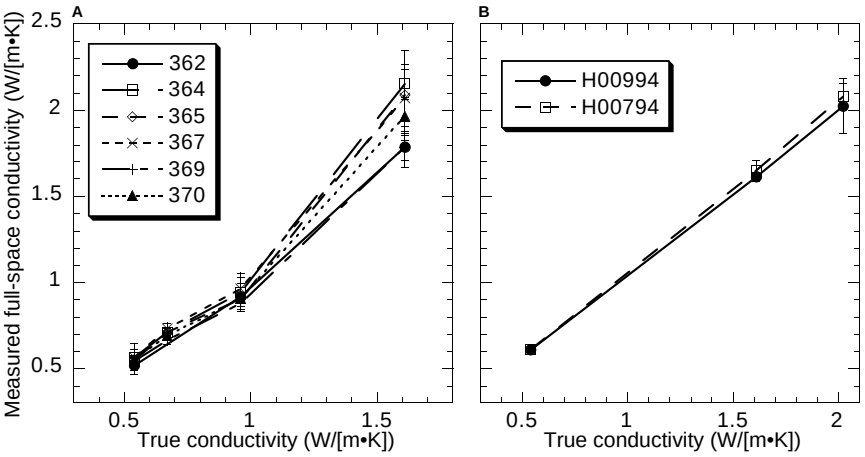

Figure 11. Measured and known thermal conductivities of standards used during Leg 170. All data are listed in Tables 12 and 13. The lines are least-squares best fits for each of the probes used. **A**. Standards for full-space probes. **B**. Standards for half-space probes.

Table 13. Calibration of full-space thermal conductivity probes.

Standard	Known conductivity (W/[m·K])	Probe 362 Mean (W/[m·K])	Probe 362 SD (W/[m·K])	Probe 362 No.	Probe 364 Mean (W/[m·K])	Probe 364 SD (W/[m·K])	Probe 364 No.	Probe 365 Mean (W/[m·K])	Probe 365 SD (W/[m·K])	Probe 365 No.
Black rubber:	0.54	0.52	0.053	6	0.565	0.045	11	0.552	0.009	12
Gelatin:	0.67	—	—	—	0.714	0.023	4	0.713	0.030	4
Red rubber:	0.96	0.918	0.077	6	0.943	0.111	3	0.903	0.028	3
Macor ceramic:	1.61	1.785	0.079	8	2.151	0.088	3	2.089	0.261	3

Standard	Known conductivity (W/[m·K])	Probe 367 Mean (W/[m·K])	Probe 367 SD (W/[m·K])	Probe 367 No.	Probe 369 Mean (W/[m·K])	Probe 369 SD (W/[m·K])	Probe 369 No.	Probe 370 Mean (W/[m·K])	Probe 370 SD (W/[m·K])	Probe 370 No.
Black rubber:	0.54	0.566	0.078	11	0.546	0.019	7	0.558	0.010	6
Gelatin:	0.67	0.735	0.031	3	0.664	0.022	3	0.692	0.019	4
Red rubber:	0.96	0.964f	0.067	3	0.882	0.020	3	0.910	0.017	3
Macor ceramic:	1.61	2.070	0.193	3	1.787	0.118	6	1.965	0.111	6

Note: SD = standard deviation, No. = number of measurements.

Table 14. Calibration of half-space thermal conductivity probes.

Standard	Known conductivity (W/[m·K])	Probe H00994 Mean (W/[m·K])	Probe H00994 SD (W/[m·K])	Probe H00994 No.	Probe H00794 Mean (W/[m·K])	Probe H00794 SD (W/[m·K])	Probe H00794 No.
Black rubber:	0.54	0.609	0.005	6	0.614	0.012	7
Macor ceramic:	1.61	1.613	0.024	6	1.651	0.057	6
Basalt:	2.024	2.024	0.159	16	2.080	0.075	7

Note: SD = standard deviation, No. = number of measurements.

probe (WSTP), and the Davis-Villinger Temperature Probe (DVTP). Techniques using the APC tool and the WSTP are similar to those used since Leg 137 (Shipboard Scientific Party, 1992b) and are described in an ODP Technical Note by Fisher and Becker (1993).

During Leg 170, the WSTP was deployed to collect bottom-water samples and to measure mudline temperatures at each drilling site. The tool, set for dual water- and temperature-sampling mode, is held for 5–15 min at 10 m above the mudline to measure the temperature of bottom water. The bottom-water sampling procedure is described in the "Geochemistry" section (this chapter).

Davis-Villinger Temperature Probe

The DVTP was deployed for the first time on Leg 164 (Shipboard Scientific Party, 1996b). The probe has a nearly cylindrical casing that terminates in a pointed tip. In situ temperatures are logged by two thermistors, one located 1 cm from the tip of the probe and the other 12 cm above the tip. A third thermistor, referred to as the internal thermistor, is located in the electronics package. Thermistor sensitivity is 1 mK in an operating range of –5°C to 20°C, and the total operating range is –5°C to 100°C. In addition to the thermistors, the probe contains an accelerometer sensitive to 0.98 m/s^2. Both peak and mean acceleration are recorded by the logger. The accelerometer data are used to track disturbances to the instrument package during the equilibration interval.

In most respects, a DVTP deployment resembles a WSTP deployment. The DVTP has several advantages over the WSTP for in situ measurements at XCB depths.

1. The geometry of the probe is nearly cylindrical, meaning that it more closely approximates a line source.
2. The taper of the probe tip is ~5°, which minimizes formation stresses associated with tool insertion.
3. The incorporation of two thermistors adds an element of reproducibility to the measurements and theoretically makes it possible to estimate the thermal gradient. In high-temperature

environments, the second thermistor can be set to allow measurements over a wider range of temperatures at reduced sensitivity.

4. The DVTP electronics are more stable than those in the WSTP, and the logger unit has greater storage capacity. The probe consumes relatively little power compared to the WSTP and has an external communication port, making it unnecessary to open the tool for data retrieval.

Shear Strength

Undrained shear strength (S_u) was determined in fine-grained plastic sediment by using the ODP motorized miniature vane shear system following ASTM D4648 Standard (ASTM, 1987). A 1.27-cm-diameter by 1.27-cm-high four-bladed vane was inserted into the working half of the split core and attached to a rotation sensor at each end of a coiled spring. A range of springs of various strengths were available. The top of the spring was rotated at a constant rate of 89°/min until the calculated torque decreased or failed to increase with additional rotation.

The instrument measures the torque and strain at the vane shaft using a torque transducer and potentiometer, respectively. The shear strength is the peak strength determined from the torque vs. strain plot. Residual shear strength was recorded unless a significant post-peak decrease in stress did not occur with additional vane rotation. Errors associated with vane shear testing include partial relief of pore pressure if the vane angular rotation rate is too slow for the sediment permeability, and cracking of the sediment during vane insertion or rotation at higher shear strengths.

Electrical Resistivity

Electrical resistivity was measured using a four-probe Wenner configuration, consisting of four 2-mm-thick stainless steel rods with an electrode spacing of 13 mm. With a Wayne-Kerr Precision Component Analyser, a 10-kHz square-wave current was applied to the outer electrodes, and the difference in potential between the two inner electrodes was measured. The size of the current was set to 10 mA. For larger currents, the measured resistivity was not stable and continued to decrease after several minutes, even in the salt-water standard.

In soft sediment where the probes were easy to insert, resistivity measurements were made approximately once per section, but less frequently in brittle material. The electrodes were pushed ~1 cm into the split-core surface. In harder sediment, a template was used to drill guide holes for the electrode pins. These holes were filled with seawater, and the core surface was then dried so that the electrodes would not communicate through the surface-water film.

To determine sediment resistivity, the measured potential was first converted to apparent resistance by dividing by the instrument current. The resistance was then converted to resistivity by multiplying by the instrument cell constant, which is defined as the cross-sectional area divided by the distance between the two voltage electrodes. The cell constant was determined by measuring the resistance of seawater in an identical split-core liner for a particular temperature, for which the resistivity is known (resistivity, c, in Ωm at temperature T in degrees Celsius is given as $c = 2.803 + 0.0996T$). The formation factor is defined as the resistivity of the sediment divided by the resistivity of the pore fluid (seawater), or alternatively the resistance of one divided by the other. As the component grains are practically nonconducting when compared with the pore fluid, the formation factor gives a measure of the volume and interconnectedness of the pore space in the sediment or rock.

Colorimetry

For a quantitative analysis of sediment color, each core was scanned at discrete intervals using a Minolta CM-2002 hand-held spectrophotometer. After the cores were split, they were covered with a thin plastic film (Glad Wrap brand) before scanning to keep the camera's lens clean. The plastic film also helped in keeping the sediments from drying too quickly. Measurements were taken every 10 cm, beginning with a control shot at 0 cm of every core and ending with another control shot recorded at the bottom of the core catcher. The control shots were taken by attaching a white calibration cap to the lens. These shots are used for qualitative analysis of instrument variability because of changes in laboratory conditions such as temperature, humidity, and background light. In addition to these control shots, for Site 1041 the instrument was also calibrated internally for white color reflectance immediately before every core was scanned.

Because the Munsell color parameters are not numerically continuous, we chose to use the L*a*b* color for the quantitative characterization of the lithostratigraphic units. The L*a*b* space is defined by the values of luminance, or lightness component (L*) and the values of the two chromatic components: the a* component, which ranges from green (–a*) to red (+a*), and the b* component, which ranges from blue (–b*) to yellow (+b*; Fig. 12).

The data obtained and processed by the spectrophotometer were written as computer files containing sample identification; L*, a*, and b*; Munsell color (hue, value, and chroma); 31 reflectance values at discrete wavelengths from 400 to 700 nm, every 10 nm; and four other values of unknown meaning. The spectral data files were concatenated in a spreadsheet, and depth below seafloor, for each sample was included in the standard ODP fashion using the corelog.dat file.

Plots of variations in L* and –a*/b* were constructed for each site. Generally, a good correlation between L* and carbonate content was found, whereas –a*/b* profiles showed other, subtle changes in lithology. Once the lithostratigraphic units were defined, statistics were performed on the spectrophotometry data to characterize the units in terms of percentage of reflectance vs. wavelength and to locate the color of the units in the L*a*b* space.

Downhole Logging

Introduction

The Borehole Research Group at the Lamont-Doherty Earth Observatory (LDEO), in conjunction with Schlumberger Well Logging Services and Schlumberger-Anadrill Drilling Services, provides the geophysical well logging aboard the *JOIDES Resolution.* Downhole logs directly determine physical and chemical properties of formations adjacent to the borehole. Interpretation of these continuous, in situ measurements yields a mineralogic, lithologic, stratigraphic, and geophysical characterization of the site. Where incomplete downhole core recovery has occurred, log data may serve as a proxy for physical properties and sedimentological data. The logs also complement

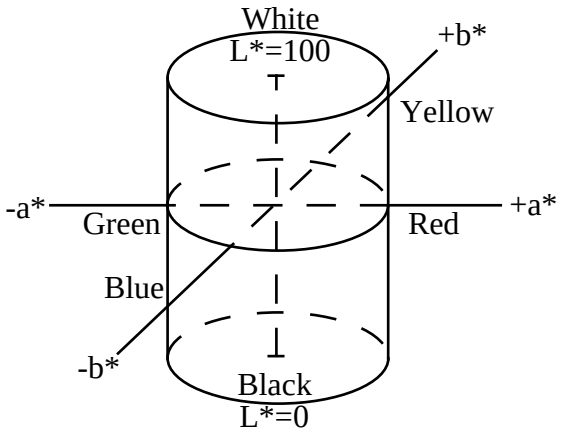

Figure 12. Spectrophotometer L*a*b color space, defined by the Commission Internationale D'Eclairage (CIE).

the discrete measurements obtained from cores, and, if successful, offer several advantages over core-based analyses in that they are rapidly collected and represent continuous, in situ measurements of the formation.

LWD operations were conducted on the *JOIDES Resolution* for the second time since Leg 156 (Shipley, Ogawa, Blum, et al., 1995). LWD allows in situ measurements immediately after the drill bit penetrates a formation, with instruments that are located at the base of the drill string. These measurements are made before the borehole is adversely affected by drilling or coring operations. In addition, LWD measurements are made while the drill string is moving, which reduces the chances of sticking and losing the BHA in a swelling clay or sloughing hole situation. LWD can also collect data open-hole in the uppermost part of the hole; this cannot by accomplished with wireline tools as the drill string is usually kept in the upper part of the borehole where hole conditions are generally bad. LWD operations on Leg 170 were complemented by wireline logging.

Logging While Drilling

The drill string was configured with the LWD tools located directly above the drill bit (Fig. 13). The Anadrill-Schlumberger tools used during LWD operations on Leg 170 consisted of a compensated dual resistivity (CDR) tool, including a spectral gamma-ray tool, and a compensated density neutron (CDN) tool (Wraight, et al., 1989; Anadrill-Schlumberger, 1993; Desbrandes, 1994). The LWD equipment is battery powered and uses electronically erasable/programmable, read-only memory chips (EPROM) downhole for nonvolatile storage

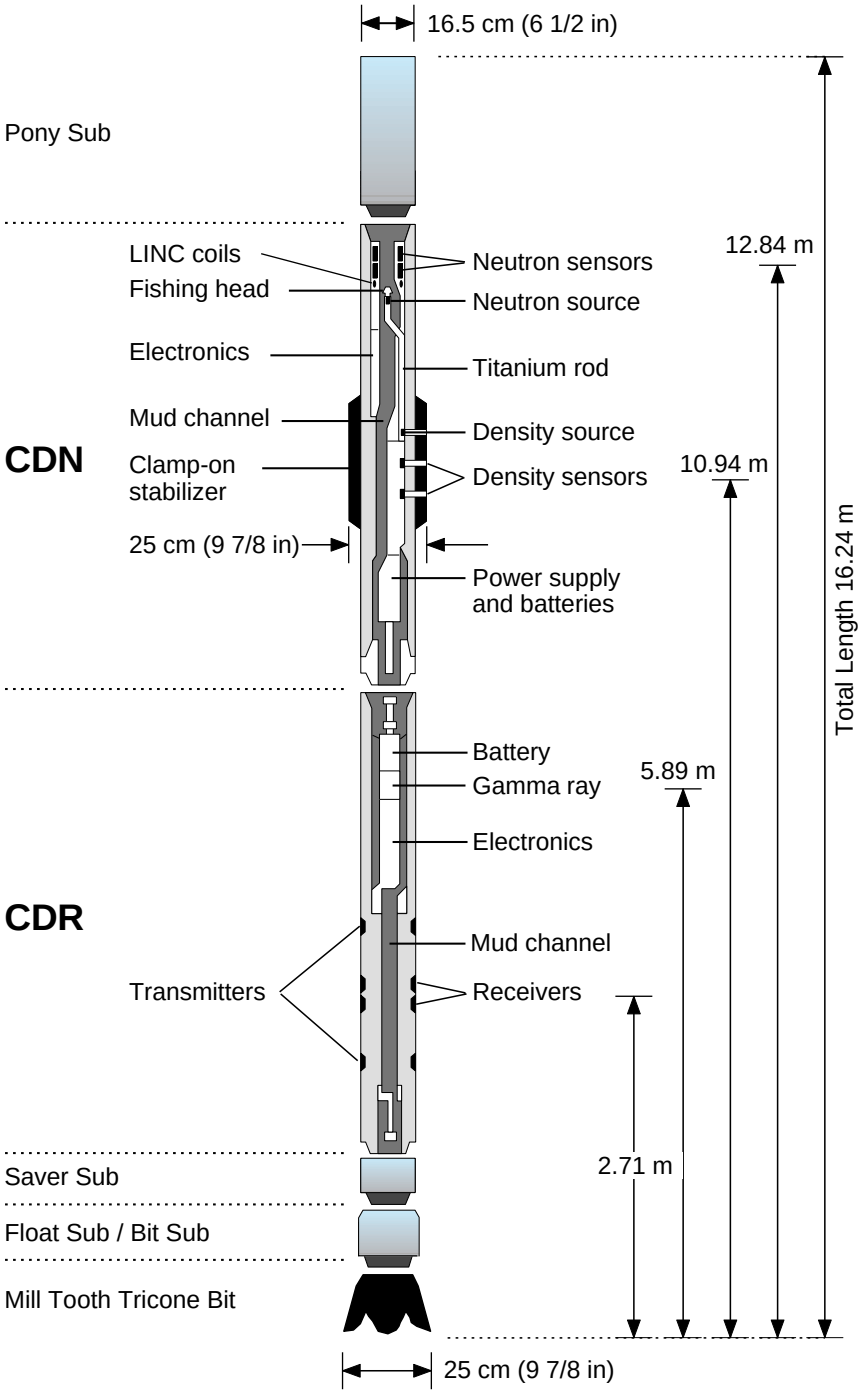

Figure 13. Position and components of compensated dual resistivity (CDR) and compensated density neutron (CDN) tools in the drill string during Leg 170 operations.

of data. The downhole data acquisition systems are synchronized with a system on the rig that monitors time and drilling depth. The tools were initialized prior to lowering of the drill string below the drillfloor. On completion of drilling, the drill string was retrieved and the data downloaded from each tool via a RS232 serial link to a PC computer. The IDEAL system (Integrated Drilling Evaluation and Logging) combines the files and generates ASCII, LIS (log information standard), and DLIS (digital log information standard) data files. The system is also used for post-acquisition data corrections and analyses.

Compensated Dual Resistivity Tool

The CDR tool is similar in principle to the conventional wireline induction tool that measures formation conductivity. Any borehole irregularities or washouts are detected by two pairs of receivers and transmitters. A 2-MHz electromagnetic wave is transmitted, and two receivers detect the phase shift (shallow measurement) and amplitude attenuation (deeper measurement) of the transmitted signal. The CDR tool includes a phase caliper that uses an algorithm to transform the phase sum and the phase shift of the two resistivity measurements into distance from the sensor. This allows correction for borehole effects and tool standoff.

The resistivity phase shift (R_{ps}) measurement is equivalent to the spherically focused log (SFL) on the induction tool. The average depth of investigation of the R_{ps} is 75 cm. The resistivity attenuation deep (R_{ad}) measurement is equivalent to the dual-induction medium measurement, with an average depth of investigation of 125 cm. The highest vertical resolution of these measurements is 15 cm.

A natural gamma-ray tool (NGT) is integrated into the CDR. Under controlled penetration rates of ~15 m/hr, reliable spectral data may be obtained. Total gamma-ray counts are binned into five energy bands to determine amounts of U, Th, and K in the formation. The NGT measures the natural radioactivity of the formation (K, U, and Th), providing both the total gamma-ray count (SGR) and a uranium-free measurement (CGR). Drilling during Leg 170 was at a controlled rate with an average rate of penetration (ROP) of 25 m/hr being achieved over the majority of the intervals drilled. This drilling proved adequate for collection of reliable spectral gamma-ray measurements, which are typically the most influenced by low count statistics at high ROPs.

Compensated Density Neutron Tool

The CDN tool is similar in principle to the wireline compensated density/compensated neutron tools. The density section of the tool uses a 1.7-curie ^{137}Cs gamma-ray source in conjunction with two gain-stabilized scintillation detectors to provide a borehole compensated density measurement. Detectors are located 7 and 14 in, respectively, below the source. The number of Compton scattering collisions (change in gamma-ray energy by interaction with the formation electrons) is related to the formation density. Returns of low-energy gamma rays provide information on the photoelectric effect (PEF), which is primarily related to lithology. The density source and detectors are positioned behind holes in the fin of a full-gauge clamp-on stabilizer (Fig. 13). This geometry forces the sensors against the borehole wall, thereby reducing the effects of borehole irregularities and drilling effects. The vertical resolution of the density and PEF measurements is about 15 cm and 5 cm, respectively.

Neutron porosity measurements are obtained using fast neutrons emitted from a 7.5-curie americium oxide-beryllium (Am-Be) source. The quantities of hydrogen in the formation primarily control the rate at which the neutrons slow down to epithermal and thermal energies. The energy of the detected neutrons has an epithermal component, because much of the incoming thermal neutron flux is absorbed as it passes through the 1-in drill collar. Neutrons are detected in near- and far-spacing detector banks, which are located 9 and 18 in, respectively, above the source. The resolution of the tool under optimum conditions is about 34 cm.

Data output from the CDN tool includes apparent neutron porosity, formation bulk density, and PEF. In addition, the CDN tool outputs a differential caliper record based on the standard deviation of density measurements made at high sampling rates around the circumference of the borehole. The measured standard deviation is compared to that of a gauge hole, and the difference is converted into amount of hole enlargement (Anadrill-Schlumberger, 1993).

Depth Control

Unlike a wireline tool, the LWD tool records data in time and does not have an exact depth reference. The depth of the LWD tool is ultimately determined by matching its times with a rig-floor system that independently records time and depth of the drill string. Although LWD depth control is well established for industry operations, LWD operations aboard the heaving platform of the *JOIDES Resolution* required special attention to depth measurements. Three optical quadrative phase shift encoders were installed on the topside drilling apparatus to measure drawwork movement, heave compensator displacement, and top drive position. Each of these sensors was carefully located and precisely calibrated to achieve high-accuracy depth measurements. Drilling parameters also collected by the surface acquisition system included uphole weight on bit, downward movement of drill pipe, pump pressure, and ROP. The combination of these parameter measurements, with precision synchronization of uphole and downhole clocks, allows the surface time/depth data and the downhole time/measurement data files to be correlated and combined after downloading the data from the LWD tools.

In addition to the depth determinations by the LWD operation, depths were monitored independently by observers in the drilling shack. Depths recorded by the LWD system, when compared with the driller's depth, varied typically by 0.1 m.

Quality Control

During the processing, quality control of the data is mainly performed by cross-correlation of all logging data. The best data are acquired in a circular borehole; this is particularly true for the density tool, which uses clamp-on stabilizers to eliminate mud standoff and to ensure proper contact with the borehole wall. A data quality indicator is given by the differential caliper (DCAL) channel which measures the tool standoff during the recording. Another quality indicator is represented by the density correction (DRHO).

Wireline Logging

Logging sensors continuously monitor geophysical, geochemical, and structural properties of the formation. Measurements are recorded typically at 15-cm depth increments. One logging string, consisting of the NGT, the general purpose inclinometry tool (GPIT), the high-temperature lithodensity tool (HLDT), the long-spaced sonic logging tool (LSS), and the phasor dual tool (DIT), was utilized during Leg 170. The vertical resolution of the NGT is ~46 cm. The GPIT determines displacement of the tool string using acceleration measurements. The HLDT measures the gamma-ray flux from a ^{137}Cs source. The source and two receivers are pressed against the borehole wall by a strong spring arm. Formation density is inferred from the gamma-ray flux by assuming that a direct relationship exists between electron density and bulk density, and that the ratio of atomic weight and atomic number for most common rock-forming elements is constant (about 2:1). The HLDT also records a PEF index, which is used as an indicator of matrix lithology that is independent of porosity. The vertical resolution of the tool is 38 cm. The LSS measures acoustic velocity of the formation between an array of transmitters and receivers separated by vertical distances ranging from 0.91 to 3.66 m.

The DIT provides three different measurements of electrical resistivity, each of which penetrates the formation to different depths and has a different vertical resolution.

Shore-Based Log Processing

Processing, quality control, and display of the logging data were performed at each of the seven holes logged during Leg 170 by the Borehole Research Group at LDEO using Schlumberger "Logos" software and additional programs developed by members of the BRG. Displays of most of these processed data are available, with accompanying text, on CD-ROM (included in the back pocket of this volume). Files of other logs (including processed temperature data and sonic waveforms) and explanatory text are included on CD-ROM (back pocket, this volume); a directory of the CD-ROM files is presented in the table of contents at the front of this volume.

Shore-based processing of the wireline data from Hole 1040C consisted of (1) depth shift to the seafloor, (2) corrections specific to certain tools, and (3) quality control and rejection of unrealistic values. Shore-based processing of the data from the remaining five holes logged with the LWD technique consisted only of depth shifting to the seafloor.

At Hole 1040C, the sonic logs have been processed to eliminate some of the noise and cycle skipping experienced during the recording. Using two sets of the four transit-time measurements and proper depth justification, four independent measurements over a 2-ft interval centered on the depth of interest are determined, each based on the difference between a pair of transmitters and receivers. The program discards any transit time that is negative or falls outside a range of meaningful values selected by the processor.

Specific tool corrections were performed on the gamma-ray data collected at Hole 1040C to account for changes in borehole size and for the composition of the drilling fluid.

Quality control was performed by cross-correlation of all logging data. If the data processor concluded that individual log measurements represented unrealistic values, the choices were to either discard the data outright and substitute the null value of "–999.25," or identify a specific depth interval containing suspect values that must be used with caution. The latter are noted in the text that accompanies all processed log displays.

In addition to the standard 15.24-cm sampling rate, bulk density data at Hole 1040C were recorded at a sampling rate of 2.54 cm. The enhanced bulk density curve is the result of a Schlumberger enhanced processing technique performed on the MAXIS system on board. Whereas in normal processing short-spacing data are smoothed to match the long-spacing ones, in enhanced processing this is reversed. In a situation where there is good contact between the HLDT pad and the borehole wall (low density correction) the results are improved, because the short-spacing data have better vertical resolution.

REFERENCES

Anadrill-Schlumberger, 1993. *Logging While Drilling:* Houston (Schlumberger), document SMP-9160.

ASTM, 1987. Standard test method for laboratory miniature vane shear test for saturated fine-grained clayey soil. In *Annual Book of ASTM Standards* (Vol. 04.08): Philadelphia (Am. Soc. Testing and Mater.).

————, 1992. Standard test method for specific gravity of soil solids by gas pycnometer. In *Annual Book of ASTM Standards* (Vol. 04.08): Philadelphia (Am. Soc. Testing and Mater.).

Baldauf, J.G., and Iwai, M., 1995. Neogene diatom biostratigraphy for the eastern equatorial Pacific Ocean, Leg 138. *In* Pisias, N.G., Mayer, L.A., Janecek, T.R., Palmer-Julson, A., and van Andel., T.H. (Eds.), *Proc. ODP, Sci. Res.*, 138: College Station, TX (Ocean Drilling Program), 105–128.

Barnes, R.O., 1988. ODP in-situ fluid sampling and measurement: a new wireline tool. *In* Mascle, A., Moore, J.C., et al., *Proc. ODP, Init. Repts.*, 110: College Station, TX (Ocean Drilling Program), 55–63.

Barron, J.A., 1985a. Late Eocene to Holocene diatom biostratigraphy of the equatorial Pacific Ocean, Deep Sea Drilling Project Leg 85. *In* Mayer, L., Theyer, F., Thomas, E., et al., *Init. Repts. DSDP,* 85: Washington (U.S. Govt. Printing Office), 413–456.

————, 1985b. Miocene to Holocene planktic diatoms. *In* Bolli, H.M., Saunders, J.B., and Perch-Nielsen, K. (Eds.), *Plankton Stratigraphy:* Cambridge (Cambridge Univ. Press), 763–809.

Berggren, W.A., Hilgen, F.J., Langereis, C.G., Kent, D.V., Obradovich, J.D., Raffi, I., Raymo, M.E., and Shackleton, N.J., 1995a. Late Neogene chronology: new perspectives in high-resolution stratigraphy. *Geol. Soc. Am. Bull.*, 107:1272–1287.

Berggren, W.A., Kent, D.V., Swisher, C.C., III, and Aubry, M.-P., 1995b. A revised Cenozoic geochronology and chronostratigraphy. *In* Berggren, W.A., Kent, D.V., Aubry, M.-P., and Hardenbol, J. (Eds.), *Geochronology, Time Scales and Global Stratigraphic Correlation*. Spec. Publ.—Soc. Econ. Paleontol. Mineral., 54:129–212.

Blow, W.H., 1969. Late middle Eocene to Recent planktonic foraminiferal biostratigraphy. *In* Brönnimann, P., and Renz, H.H. (Eds.), *Proc. First Int. Conf. Planktonic Microfossils, Geneva, 1967:* Leiden (E.J. Brill), 1:199–422.

Boyce, R.E., 1973. Physical properties—methods. *In* Edgar, N.T., Saunders, J.B., et al., *Init. Repts. DSDP,* 15: Washington (U.S. Govt. Printing Office), 1115–1128.

————, 1976. Definitions and laboratory techniques of compressional sound velocity parameters and wet-water content, wet-bulk density, and porosity parameters by gravimetric and gamma-ray attenuation techniques. *In* Schlanger, S.O., Jackson, E.D., et al., *Init. Repts. DSDP,* 33: Washington (U.S. Govt. Printing Office), 931–958.

Brown, K.M., and Ransom, B., 1996. Porosity corrections for smectite-rich sediments: impact on studies of compaction, fluid generation, and tectonic history. *Geology,* 24:43–84.

Burckle, L.H., 1972. Late Cenozoic planktonic diatom zones from the eastern equatorial Pacific. *In* Simonsen, R. (Ed.), *First Symposium on Recent and Fossil Marine Diatoms.* Nova Hedwegia Beih., 39:217–246.

————, 1977. Pliocene and Pleistocene diatom datum levels from the equatorial Pacific. *Quat. Res.*, 7:330–340.

————, 1978. Early Miocene to Pliocene diatom datum level for the equatorial Pacific. *Proc. Second Working Group Mtg. Biostratigraphic Datum Planes, Pacific Neogene, IGCP Proj. 114.* Spec. Publ., Geol. Res. Dev. Ctr., 1:25–44.

Cannat, M., Karson, J.A., Miller, D.J., et al., 1995. *Proc. ODP, Init. Repts.*, 153: College Station, TX (Ocean Drilling Program).

Davis, E.E., Fisher, A.T., Firth, J.V., et al., 1997. *Proc. ODP, Init. Repts.*, 168: College Station, TX (Ocean Drilling Program).

Desbrandes, R., 1994. *Data Acquisition and Processing While Drilling.* Louisiana State Univ.

Emeis, K.-C., and Kvenvolden, K.A., 1986. Shipboard organic geochemistry on *JOIDES Resolution. ODP Tech. Note,* 7.

Espitalié, J., Deroo, G., and Marquis, F., 1986. La pyrolyse Rock-Eval et ses applications, Partie III. *Rev. Inst. Fr. Pet.*, 41:73–89.

Fisher, A., and Becker, K., 1993. A guide to ODP tools for downhole measurements. *ODP Tech. Note,* 10.

Gieskes, J.M., Gamo, T., and Brumsack, H., 1991. Chemical methods for interstitial water analysis aboard *JOIDES Resolution. ODP Tech. Note,* 15.

Gillis, K., Mével, C., Allan, J., et al., 1993. *Proc. ODP, Init. Repts.*, 147: College Station, TX (Ocean Drilling Program).

Hay, W.W., 1970. Calcareous nannofossils from cores recovered on Leg 4. *In* Bader, R.G., Gerard, R.D., et al., *Init. Repts. DSDP,* 4: Washington (U.S. Govt. Printing Office), 455–501.

Hoppie, B.W., Blum, P., and the Shipboard Scientific Party, 1994. Natural gamma-ray measurements on ODP cores: introduction to procedures with examples from Leg 150. *In* Mountain, G.S., Miller, K.G., Blum, P., et al., *Proc. ODP, Init. Repts.*, 150: College Station, TX (Ocean Drilling Program), 51–59.

Kennett, J.P., and Srinivasan, M.S., 1983. *Neogene Planktonic Foraminifera: A Phylogenetic Atlas:* Stroudsburg, PA (Hutchinson Ross).

Lundberg, N., and Moore, J.C., 1986. Macroscopic structural features in Deep Sea Drilling Project cores from forearc regions. *In* Moore, J.C. (Ed.), *Structural Fabric in Deep Sea Drilling Project Cores From Forearcs.* Mem.—Geol. Soc. Am., 166:13–44.

Manheim, F.T., and Sayles, F.L., 1974. Composition and origin of interstitial waters of marine sediments, based on deep sea drill cores. *In* Goldberg,

E.D. (Ed.), *The Sea* (Vol. 5): *Marine Chemistry: The Sedimentary Cycle:* New York (Wiley), 527–568.

Martini, E., 1971. Standard Tertiary and Quaternary calcareous nannoplankton zonation. *In* Farinacci, A. (Ed.), *Proc. 2nd Int. Conf. Planktonic Microfossils Roma:* Rome (Ed. Tecnosci.), 2:739–785.

Mazzullo, J., and Graham, A.G. (Eds.), 1988. *Handbook for Shipboard Sedimentologists.* ODP Tech. Note, 8.

McKenzie, W.S., Donaldson, C.H., and Guilford, C., 1982. *Atlas of Igneous Rocks and Their Textures:* New York (Longman Scientific & Technical; Wiley.)

Ratcliffe, E.H., 1960. Thermal conductivities of ocean sediments. *J. Geophys. Res.*, 65:1535–1541.

Rothwell, R.G., 1989. *Minerals and Mineraloids in Marine Sediments: An Optical Identification Guide:* Basking, UK (Elsevier Appl. Sci. Publ.).

Schultheiss, P.J., and McPhail, S.D., 1989. An automated *P*-wave logger for recording fine-scale compressional wave velocity structures in sediments. *In* Ruddiman, W., Sarnthein, M., et al., *Proc. ODP, Sci. Results,* 108: College Station, TX (Ocean Drilling Program), 407–413.

Shackleton, N.J., Baldauf, J.G., Flores, J.-A., Iwai, M., Moore, T.C. Jr., Raffi, I., and Vincent, E., 1995. Biostratigraphic summary for Leg 138. *In* Pisias, N.G., Mayer, L.A., Janecek, T.R., Palmer-Julson, A., and van Andel, T.H. (Eds.) *Proc. ODP, Sci. Results,* 138: College Station, TX (Ocean Drilling Program), 517–536.

Shipboard Scientific Party, 1992a. Explanatory notes. *In* Davis, E.E., Mottl, M.J., Fisher, A.T., et al., *Proc. ODP, Init. Repts.,* 139: College Station, TX (Ocean Drilling Program), 55–97.

————, 1992b. Introduction and explanatory notes. *In* Becker, K., Foss, G., et al., *Proc. ODP, Init. Repts.,* 137: College Station, TX (Ocean Drilling Program), 5–12.

————, 1995. Explanatory notes. *In* Shipley, T.H., Ogawa, Y., Blum, P., et al., *Proc. ODP, Init. Repts.,* 156: College Station, TX (Ocean Drilling Program), 39–68.

————, 1996a. Explanatory notes. *In* Jansen, E., Raymo, M.E., Blum, P., et al., *Proc. ODP, Init. Repts.,* 162: College Station, TX (Ocean Drilling Program), 21–45.

————, 1996b. Explanatory notes. *In* Paull, C.K., Matsumoto, R., Wallace, P.J., et al., *Proc. ODP, Init. Repts.,* 164: College Station, TX (Ocean Drilling Program), 13–41.

Shipley, T.H., Ogawa, Y., Blum, P., et al., 1995. *Proc. ODP, Init. Repts.,* 156: College Station, TX (Ocean Drilling Program).

Sperner, B., Ott, R., and Ratschbacher, L., 1993. Fault-striae analysis: a turbo PASCAL program packet for graphical presentation and reduced stress-tensor calculation. *Comput. Geosci.,* 19:1361–1388.

Streckeisen, A., 1974. Classification and nomenclature of plutonic rocks. *Geol. Rundsch.,* 63:773–786.

Tissot, B.P., and Welte, D.H., 1984. *Petroleum Formation and Occurrence* (2nd ed.): Heidelberg (Springer-Verlag).

Vacquier, V., 1985. The measurement of thermal conductivity of solids with a transient linear heat source on the plane surface of a poorly conducting body. *Earth Planet. Sci. Lett.,* 74:275–279.

von Herzen, R.P., and Maxwell, A.E., 1959. The measurement of thermal conductivity of deep-sea sediments by a needle-probe method. *J. Geophys. Res.,* 64:1557–1563.

Westbrook, G.K., Carson, B., Musgrave, R.J., et al., 1994. *Proc. ODP, Init. Repts.,* 146 (Pt. 1): College Station, TX (Ocean Drilling Program).

Wraight, P., Evans, M., Marienback, E., Rhein-Knudsen, E.M., and Best, D., 1989. Combination formation density and neutron porosity measurements while drilling. *Trans. SPWLA 30th Ann. Logging Symp.,* Denver.

MS 170IR-102